

Intracellular Transport of Vaccinia Virus in HeLa Cells Requires WASH-VPEF/FAM21-Retromer Complexes and Recycling Molecules Rab11 and Rab22

Jye-Chian Hsiao,^a Li-Wei Chu,^{d,e} Yung-Tsun Lo,^a Sue-Ping Lee,^b Tzu-Jung Chen,^c Cheng-Yen Huang,^a Yueh-Hsin Ping,^{d,e,f,g,h} Wen Chang^{a,c}

Institute of Molecular Biology^a and Imaging Core, Institute of Molecular Biology,^b Academia Sinica, and Institute of Genome Sciences,^c Department and Institute of Pharmacology,^d Institute of Biophotonics,^e Biophotonics and Molecular Imaging Research Center,^f VYM Genome Research Center,^g and Infection and Immunity Research Center,^h National Yang-Ming University, Taipei, Taiwan, Republic of China

ABSTRACT

Vaccinia virus, the prototype of the *Orthopoxvirus* genus in the family *Poxviridae*, infects a wide range of cell lines and animals. Vaccinia mature virus particles of the WR strain reportedly enter HeLa cells through fluid-phase endocytosis. However, the intracellular trafficking process of the vaccinia mature virus between cellular uptake and membrane fusion remains unknown. We used live imaging of single virus particles with a combination of various cellular vesicle markers, to track fluorescent vaccinia mature virus particle movement in cells. Furthermore, we performed functional interference assays to perturb distinct vesicle trafficking processes in order to delineate the specific route undertaken by vaccinia mature virus prior to membrane fusion and virus core uncoating in cells. Our results showed that vaccinia virus traffics to early endosomes, where recycling endosome markers Rab11 and Rab22 are recruited to participate in subsequent virus trafficking prior to virus core uncoating in the cytoplasm. Furthermore, we identified WASH-VPEF/FAM21-retromer complexes that mediate endosome fission and sorting of virus-containing vesicles prior to virus core uncoating in the cytoplasm.

IMPORTANCE

Vaccinia mature virions of the WR strain enter HeLa cells through fluid phase endocytosis. We previously demonstrated that virus-containing vesicles are internalized into phosphatidylinositol 3-phosphate positive macropinosomes, which are then fused with Rab5-positive early endosomes. However, the subsequent process of sorting the virion-containing vesicles prior to membrane fusion remains unclear. We dissected the intracellular trafficking pathway of vaccinia mature virions in cells up to virus core uncoating in cytoplasm. We show that vaccinia mature virions first travel to early endosomes. Subsequent trafficking events require the important endosome-tethered protein VPEF/FAM21, which recruits WASH and retromer protein complexes to the endosome. There, the complex executes endosomal membrane fission and cargo sorting to the Rab11-positive and Rab22-positive recycling pathway, resulting in membrane fusion and virus core uncoating in the cytoplasm.

Vaccinia virus is the prototype of the *Orthopoxvirus* genus in the family *Poxviridae*, which includes the variola virus that causes smallpox diseases. It has a broad host range and infects a wide variety of cell lines and animals. Vaccinia virus produces two forms of infectious virions, mature virus (MV) and extracellular virus (EV), which contain different membrane proteins (1). MV particles are abundant in infected cells and contain ~80 viral proteins (2, 3), which contribute to the complex virus entry processes that reportedly vary among different cells and virus strains (4–12).

In HeLa cells, vaccinia MV initially attaches to cellular surface component glycosaminoglycans (13–15) and the extracellular matrix protein laminin (16). MV particles then cluster at plasma membrane lipid rafts (17) where the virus further interacts with integrin $\beta 1$ (18) and CD98 receptor molecules (19) that facilitate PI-3K/Akt activation and actin-dependent endocytosis (20, 21). MV membranes are rich in phosphatidylserine (PS); thus, it was proposed that MV may mimic apoptotic bodies during cell entry (21, 22). However, Laliberte and Moss demonstrated that phospholipids other than PS could also reconstitute MV infectivity (23). To date, there is no evidence that any particular PS receptor is required for vaccinia MV entry (24–26).

Following internalization into cells, the vaccinia virus MV-containing vesicles are internalized into CD98-positive and phos-

phatidylinositol 3-phosphate (PI3P)-positive macropinosomes and subsequently fused with Rab5-positive early endosomes (19). However, little is known about the process of sorting the MV-containing vesicles in cells prior to membrane fusion. In the present study, we dissect the intracellular trafficking pathway of vaccinia MV and demonstrate a role of the cellular WASH-VPEF/

Received 27 January 2015 Accepted 26 May 2015

Accepted manuscript posted online 3 June 2015

Citation Hsiao J-C, Chu L-W, Lo Y-T, Lee S-P, Chen T-J, Huang C-Y, Ping Y-H, Chang W. 2015. Intracellular transport of vaccinia virus in HeLa cells requires WASH-VPEF/FAM21-retromer complexes and recycling molecules Rab11 and Rab22. *J Virol* 89:8365–8382. doi:10.1128/JVI.00209-15.

Editor: G. McFadden

Address correspondence to Wen Chang, mbwen@ccvax.sinica.edu.tw, or Yueh-Hsin Ping, yhpingleym.edu.tw.

J.-C.H., L.-W.C., and Y.-T.L. contributed equally to this article.

Supplemental material for this article may be found at <http://dx.doi.org/10.1128/JVI.00209-15>.

Copyright © 2015, American Society for Microbiology. All Rights Reserved.

doi:10.1128/JVI.00209-15

FAM21-retromer complex in vaccinia virus trafficking through the early endosome-recycling pathway.

MATERIALS AND METHODS

Cells, viruses, plasmid vectors, and reagents. HeLa cells were cultured in Dulbecco modified Eagle medium (DMEM) supplemented with 10% fetal bovine serum and 2% penicillin-streptomycin (Sigma). The wild-type (WT) vaccinia virus of the Western Reserve (WR) strain, the WR-ΔA26L deletion mutant virus, and the recombinant WR virus expressing a mcherry-A4 fusion protein (WR-A4-mCherry) were described previously (20, 27). WR virus expressing a CFP-A4 fusion protein (WR-A4-CFP) was constructed and purified similar to that of WR-A4-mCherry. MV particles were harvested from BSC40 cells and purified by CsCl gradient centrifugation as previously described (28).

The plasmids pEGFP-C3-Rab5, pEGFP-C3-Rab5Q79L, and pEGFP-C3-Rab5S34N were provided by Marino Zerial (Max Planck Institute, Germany). The plasmids pEGFP-Rab22a, pEGFP-Rab22aQ64L, and pEGFP-Rab22aS19N were gifts from Julie Donaldson (National Institutes of Health, Bethesda, MD). The plasmids pIRES neo3-Pcmv-GFP-hVPS35, pIRES neo3-Pcmv-GFP-hVPS-26, and pIRES neo3-Pcmv-GFP-hVPS-29 were provided by Mitsuaki Tabuchi (Kagawa University, Japan) (29). The Rab7 and Rab11 plasmids were purchased from the Missouri S&T cDNA Resource Center (Rolla, MO). The plasmids pEGFP-C1-Rab34, pEGFP-C1-Rab34Q11L, and pEGFP-C1-Rab34T66N were provided by Takeshi Endo (Department of Biology, Chiba University, Chiba, Japan). The expression plasmids CFP-Rab7Q70L, CFP-Rab7T22N, GFP-Rab11Q70L, and GFP-Rab11S25N were generated through *in vitro* mutagenesis using the wild-type plasmids CFP-Rab7 and GFP-Rab11 as the templates with the QuikChange site-directed mutagenesis kit as previously described (30, 31). To facilitate three-dimensional (3D) imaging, we also generated three constructs that express mCherry protein fused in-frame with wild-type Rab11, Rab11Q70L, and Rab11S25N cDNA, respectively. Antibodies against EEA1 and mannose-6 phosphate receptor were purchased from BD Biosciences and NOVUS, Inc., respectively. Anti-Vps35 antibody was obtained from Imgenex. Antibody against cyclophilin B (CypB) was purchased from Santa Cruz. Antibodies against WASH and actin were purchased from Sigma. Rabbit anti-vaccinia virus A4 and anti-VPEF antibodies were previously described (20). Tetramethylrhodamine-conjugated goat anti-Rabbit and anti-mouse IgG antibodies were purchased from Invitrogen, Inc. Cy5-conjugated goat anti-Rabbit IgG antibody was purchased from Jackson ImmunoResearch Laboratories, Inc. Texas Red-conjugated transferrin and Texas Red-conjugated dextran were purchased from Molecular Probes and Invitrogen, Inc. Lipofectamine and Plus reagent were purchased from Invitrogen, Inc. The QuikChange site-directed mutagenesis kit was purchased from Stratagene, Inc.

In vitro mutagenesis of Rab7 and Rab11 mutant plasmids. To generate mutant Rab7 and Rab11 plasmids expressing CFP-Rab7Q70L, CFP-Rab7T22N, GFP-Rab11Q70L, and GFP-Rab11S25N (30, 31), we performed *in vitro* mutagenesis using a QuikChange site-directed mutagenesis kit. The wild-type plasmids CFP-Rab7 and GFP-Rab11 were used as the templates. Mutagenesis was performed using the following primer pairs: for CFP-Rab7Q70L, 5'-ATATGGGACACAGCAGGACTGGAACCGTTCCAGTCCTGCTGTCCCATAAT-3' and 5'-GAGAGACTGGAAACCGTTCCAGTCCTGCTGTCCCATAAT-3'; for CFP-Rab7T22N, 5'-GATTCTGGAGTCGGGAAGAACTCACTCATGAACCAGTAT-3' and 5'-ATACTGGTCATGAGTGAGTTCTTCCGACTCCAGAACATC-3'; for GFP-Rab11Q70L, 5'-ATATGGGACACAGCAGGGCTAGAGCGATATCGAGCTATA-3' and 5'-TATAGCTCGATATCGCTCTAGCCCTGCTGTGTCCTCATAT-3'; and for GFP-Rab11S25N, 5'-GATTCTGGTGTGAAAGAATAATCCCTGTCTCGATTT-3' and 5'-AAATCGAGACAGGAGATTATTCTTCCAACACCCAGAAATC-3'. The sequences of the mutant DNA fragments were confirmed by DNA sequencing.

siRNA knockdown experiments. We purchased from MDBio, Inc. (Taiwan), small interfering RNA (siRNA) duplexes targeting CypB—WASH (CCGCCACAGGAUCCAGAGCAA), Vps26 (AACUCUGUAA CCCUUGAG), Vps35 (GCCUUCAGAGGAUGUUGUAUCUUUA), and

Snx1 (CCACGUGAUCAAGUACCUU)—as previously described (29, 32, 33). Knockdown experiments were performed as previously reported (20). In brief, HeLa cells were either mock transfected (Si-control) or transfected with 20 nM siRNA duplex—e.g., CypB (Si-CypB), Vps26 (Si-Vps26), Vps35 (Si-Vps35), Snx1 (Si-Snx1), or WASH (Si-WASH)—using Lipofectamine 2000 (Invitrogen) according to the manufacturer's instructions. The cells were harvested for immunoblots, quantitative PCR, and virus uncoating assays as previously described (20).

Single-particle tracking imaging analyses. Tracking experiments were performed as previously described (34) with minor modifications. In brief, 2×10^5 HeLa cells were seeded in a 35-mm glass-bottom culture dish (MatTek, USA) and incubated overnight at 37°C. HeLa cells were transfected with the plasmid GFP-Rab5, GFP-Rab11, GFP-Rab22, or CFP-Rab7 using Lipofectamine 2000 (Invitrogen). After 24 h, HeLa cells were infected with WR-A4-mCherry MV in PBS-AM buffer (phosphate-buffered saline, 0.05% bovine serum albumin [BSA], and 10 mM MgCl₂) at a multiplicity of infection (MOI) of 10 PFU/cell and incubated for 30 min at 4°C to synchronize virus binding. The cells were then washed once with PBS, replenished with phenol red-free DMEM, and placed on a 37°C heated stage. Images of living cells were recorded using an inverted microscope (IX 71; Olympus, Japan) equipped with the live cell instrument (Leica, Germany) with 5% CO₂ supplement, an imaging split system (U-SIP; Olympus), and a high-sensitivity monochrome charge-coupled device (CCD) camera (CoolSNAP HQ2; Photometrics, USA). Cells were visualized using a 100× 1.4 NA oil-immersion objective lens. Fluorescent images were recorded by exciting green fluorescent protein (GFP) with a 488-nm Ti-Sapphire laser (Coherent, USA) and by exciting mCherry with a 532-nm DPSS laser (Onset-EO, Taiwan). The fluorescent emission was spectrally separated by 550-nm long-pass dichroic mirrors (Chroma, Rockingham, VT) and imaged onto two separate areas of the CCD camera. A 632/60 nm band-pass filter was used for mCherry emission, and a 510/20-nm band-pass filter was used for GFP emission. Time-lapse image sequences were recorded using RS Image (v1.9.2; Roper Scientific, Inc., USA).

Quantification of image analysis. Image analysis and single-particle tracking described above were performed using Meta Imaging Series 7.7 (MetaMorph, USA). The process of tracking virus particle position was previously described (35), as implemented in a Matlab-based Polyparticletracker program. Image noise was first reduced and smoothed by convolving the image with a Gaussian function. Single particles were then tracked and particle center coordinates were estimated. Next, subpixel refinement of the particle was coordinated by polynomial fitting with Gaussian weight (PFGW). Particle discrimination and parameters were subsequently calculated. Finally, the particle positions were connected between individual frames by straight lines, forming the particle trajectories using the Polyparticletracker program (35). Using the ImageJ program, colocalization of a virus particle with a fluorescent cellular marker was confirmed if both images showed an apparent overlap on the focal plane and a close trajectory during the tracking time interval. Tracking events were collected from ≥150 individual virus particles in at least three independent experiments. Statistical significance was determined by using a Student *t* test, with *P* < 0.05 considered significant.

3D tracking imaging analyses. The tracking experiments were performed as previously described (34) with minor modification. In brief, 2×10^5 HeLa cells were seeded in a 35-mm glass-bottom culture dish (MatTek) and incubated at 37°C overnight. HeLa cells were transfected with an individual plasmid or in a combination of two plasmids of mCherry-Rab5, GFP-Rab22, and GFP-Rab11 by Lipofectamine 2000 (Invitrogen). After 24 h, HeLa cells were infected with WR-A4-CFP MV in PBS-AM buffer (PBS, 0.05% BSA, 10 mM MgCl₂) at an MOI of 10 PFU/cell at 4°C for 30 min to synchronize virus binding. The cells were then washed once with PBS, replenished with growth media, and placed on a heated stage at 37°C. Images were acquired using a spinning disk confocal imaging system (Revolution WD Confocal System; Andor Technology) mounted on a Nikon inverted microscope (Eclipse Ti) equipped with a

Nikon Plan Apo λ 100 \times oil immersion objective lens with an NA of 1.45 and an electron multiplication charge-coupled device camera (EMCCD). To capture a simultaneous image of A4-CFP MV particles with both GFP-tagged and mCherry-tagged Rab proteins, CFP was excited with a 445-nm laser, GFP was excited with a 488-nm laser, and mCherry was excited with a 561-nm laser. 3D images were acquired using the maximum z-projection of the confocal z-stacks with 10 z-section images per min. Imaging processing and analyses were used by using the image software Imaris 8.0.1 (Bitplane, United Kingdom).

Virus core uncoating assay. HeLa cells were seeded onto coverslips 24 h prior to transfection. The next day, cells were transfected with the wild-type, GTP-bound, or GDP-bound form of the Rab GTPase plasmids and incubated for another 20 to 24 h. These cells were subsequently infected with vaccinia virus MV, and the level of virus entry was analyzed using viral core uncoating assays, which was initially described by Vanderplaschen et al. (11) and modified by Huang et al. and Senkevich et al. (20, 36). Briefly, HeLa cells were infected with the wild-type WR or WR Δ A26L virus at an MOI of 40 PFU/cell through 1 h of incubation at 4°C. The cells were then washed three times with PBS and incubated for 2 h at 37°C in the presence of cycloheximide (15 μ g/ml). Alternatively, HeLa cells were treated with dimethyl sulfoxide (DMSO) or with 25 nM baflomycin A (BFLA) for 30 min and subsequently infected with wild-type WR or WR Δ A26L virus at 37°C for 60 min. After being washed with phosphate-buffered saline (PBS), the cells were incubated in growth medium with or without BFLA for 2 h at 37°C. The cells were then fixed with 4% paraformaldehyde, permeabilized in PBS–0.2% saponin and BSA, and stained with rabbit anti-A4L antibody, followed by rhodamine-conjugated goat anti-rabbit IgG antibody and 0.5 μ g of DAPI (4',6'-diamidino-2-phenylindole)/ml. Cell images were collected using a LSM780 confocal laser scanning microscope (Carl Zeiss, Germany) equipped with a 63 \times objective lens and confocal microscopy software (Zen 2009; Carl Zeiss). The fluorescent particles from multiple z-section images were counted, and the average numbers of uncoated cores per cell were determined as described previously (20).

Ligand and antibody internalization assay. HeLa cells were seeded onto coverslips 24 h prior to transfection. The next day, the cells were transfected with the wild-type, GTP-bound, or GDP-bound form of the Rab GTPase plasmids, followed by another 20 to 24 h of incubation. For manose-6-phosphate receptor (CI-MPR) uptake, HeLa cells were incubated for 1 h with 10 μ g of CI-MPR/ml at 37°C. The cells were then fixed, permeabilized in PBS–0.2% saponin and BSA, and stained with rhodamine-conjugated goat anti-mouse IgG antibody for confocal microscopy analyses as previously described (37). For dextran uptake, HeLa cells were incubated with 5 μ g of Texas Red-conjugated dextran/ml for 1 h at 37°C. The cells were then washed three times with PBS, followed by incubation for 15 min at 37°C in complete medium, followed in turn by fixation for confocal microscopy analyses as previously described (20). Cells were stained with anti-VPEF antibody (1:1,000), followed by Cy5-conjugated anti-rabbit antibody. DNA was stained with 0.5 μ g of DAPI/ml. Cell images were collected using an LSM780 confocal laser scanning microscope (Carl Zeiss) with either a 40 \times or 63 \times objective lens.

RESULTS

Vaccinia MV transports to early endosomes after internalization. Fluorescent vaccinia WR-A4-mCherry MV particles were purified and used to infect HeLa cells expressing wild-type GFP-Rab5 protein that marks early endosomes in cells. The movement of the fluorescent viral particles was then monitored using live-imaging microscopy (Fig. 1A; see also Movie S1 in the supplemental material). Trajectory tracing of MV and endosome movement revealed a nonstochastic association between the two, indicating that MV traveled with the early endosome (Fig. 1B). The association of MV with endosomes was kinetically regulated. For simplicity, we divided all of the particle-endosome colocalization events

into two phases of viral infection: early (<45 min) and late (>45 min). Single virus particle tracking (of >150 particles) showed that more vaccinia MV particles became colocalized with Rab5-positive early endosomes in the early phase after viral infection (~32.0%) than in the late phase (~14%) (Fig. 1C). The present live imaging data were in agreement with our previous data obtained from paraformaldehyde-fixed cells, showing the transport of internalized MV from PI3P-positive macropinosomes to Rab5-positive early endosomes (19). Despite these consistent results in quantification analyses, one may be concerned that conventional wide-field fluorescence microscopy is limited in optical resolution due to fluorescence interference. To further illustrate the trafficking behavior of MV with early endosomes in 3D within a cell, 3D dual-color time-lapse tracking using spinning-disk confocal microscopy was performed. A typical example of MV endocytic trafficking itinerary showed that this particular virus particle colocalized with a Rab5-positive endosome at 7 min postinfection and cotrafficked until 14 min postinfection, as shown by the colocalization of MV and Rab5 (Fig. 1D). These results indicated that the endocytic trafficking of a single MV particle indeed moved toward an early endosome. A three-dimensional trajectory of MV intracellular trafficking with a Rab5-positive endosome is shown in Movie S2 in the supplemental material.

We next used two dominant-negative Rab5 mutants—the GTP-bound Rab5Q79L and GDP-bound Rab5S34N—to interfere with fusion and fission in early endosome function. To assess the inhibitory effect of Rab5 mutants on vaccinia MV entry, we chose to perform virus uncoating assays which measured viral cores that are released into cytoplasm after membrane fusion, as previously described (11, 20, 36). We consider virus core uncoating is an immediate readout of successful MV membrane fusion and is better than DiD quenching analysis, which measures hemifusion, or viral early gene expression, which is downstream of virus uncoating in cytoplasm. HeLa cells were transfected with either wild-type GFP alone, GFP-Rab5, GFP-Rab5Q79L, or GFP-Rab5S34N and infected with WT-WR MV. Expression of GFP or GFP-Rab5 did not inhibit viral core uncoating in cytoplasm, whereas the expression of Rab5Q79L and Rab5S34N specifically reduced vaccinia virus uncoating (Fig. 2A and B). Similar results were obtained with viral luciferase assays (data not shown). To ensure that expression of Rab5Q79L and Rab5S34N did not affect the initial attachment of vaccinia MV to cells, we performed fluorescence-activated cell sorting (FACS) analyses to quantify the amount of vaccinia MV bound to HeLa cells that express wild-type GFP alone, GFP-Rab5, GFP-Rab5Q79L, or GFP-Rab5S34N (Fig. 2C). We also measured the level of integrin β 1 and CD98 on plasma membrane of these fluorescence-positive cells (Fig. 2C). The histograms showed that expression of GFP-Rab5Q79L or GFP-Rab5S34N did not reduce the level of these two cellular receptors on plasma membrane (Fig. 2D), as well as the amount of vaccinia MV binding to cells (Fig. 2E). Taken together, the data showed that vaccinia MV traffics through early endosomes prior to core uncoating in the cytoplasm.

WASH, a protein that mediates actin polymerization and cargo sorting at early endosomes, is also required for vaccinia WR-MV transport. We previously showed that VPEF is not required for vaccinia MV binding to cells but is required for endocytosis of vaccinia MV of the WT-WR strain (20, 38). Although we initially thought the protein was expressed on cell surface (38) overexpression of GFP-VPEF in HeLa cells and immunofluores-

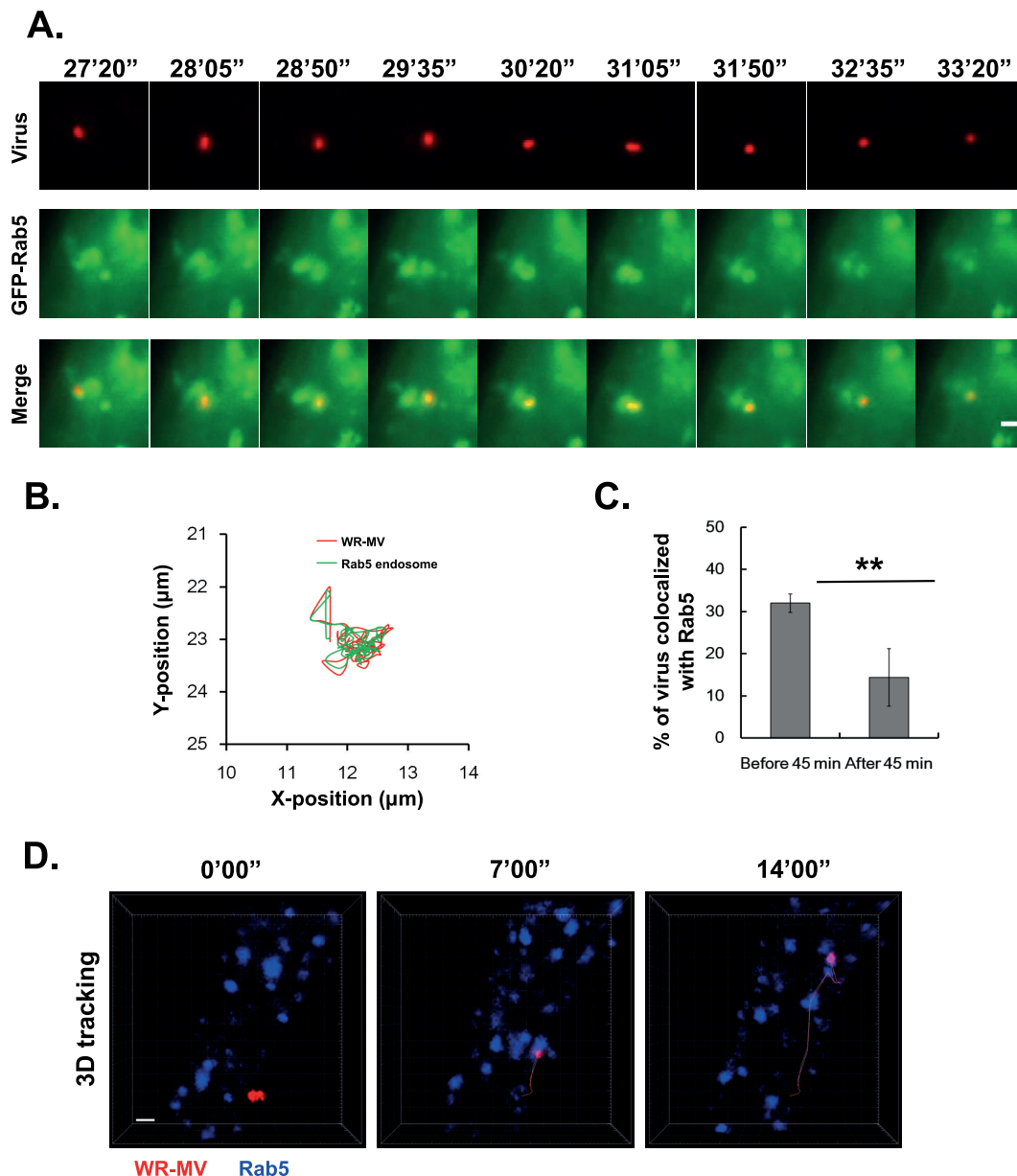


FIG 1 Single-particle tracking reveals vaccinia MV colocalized with early endosomes. (A) The represented frames show the endocytic trafficking behavior of a single fluorescent vaccinia WR-A4-mCherry MV particle that was colocalized with the GFP-Rab5 endosome in HeLa cells transiently expressing GFP-Rab5. A4-mCherry MV particles are displayed in red (top panel); GFP-Rab5 endosomes are shown in green (middle panel), and vesicles containing both the A4-mCherry MV particle and the GFP-Rab5 endosome are shown in yellow (bottom panel). The scale bar at the bottom of the right panel represents 1 μm in length. (B) The overlapped trajectory profiles of the A4-mCherry MV particle (red) and GFP-Rab5 endosome (green) in HeLa cells were determined using Polyparticletracker (35). (C) The histogram represents the colocalization of A4-mCherry MV particles and Rab5-positive endosomes. A total of 181 events were recorded, and the data shown are from three independent replicates. Statistical significance was determined using Student *t* test. **, $P < 0.01$. (D) Cotrafficking of MV particle (in red) with a Rab5-positive (in blue) endosome, as revealed by 3D time-lapse tracking with a spinning disk confocal microscopy. The selected time frames show the 3D trafficking behavior of a single A4-CFP MV particle and the Rab5-positive endosomes in a cell. The scale bar represents 1 μm in length. The Rab5-positive endosome and A4-CFP MV in 3D trajectory are shown in Movie S2 in the supplemental material.

cence staining of endogenous VPEF in HeLa cells revealed that a majority of VPEF protein exists as intracellular speckles in cytoplasm (20). To demonstrate a specific role of VPEF in vaccinia virus endocytosis, we performed an acid-bypass infection experiment in which cell-bound WR-MV particles were treated with acidic buffer to force virus membranes to directly fuse with plasma membrane (4, 27). We anticipated that, in this situation, VPEF

would no longer be required for WT-WR MV entry. Indeed, our results showed that at neutral pH, WT-WR MV entry into HeLa cells occurred through a BFLA-sensitive endocytic process and was reduced by knockdown of VPEF, but not CypB (Fig. 3A and B). However, at low pH, WT-WR entry into HeLa cells became BFLA resistant, and VPEF knockdown had no effect on WR-MV entry through plasma membrane fusion (Fig. 3C). We also per-

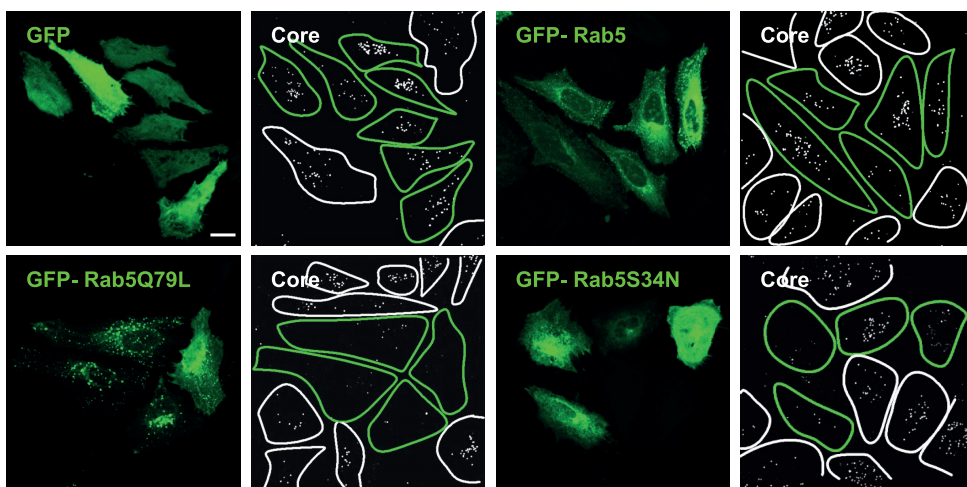
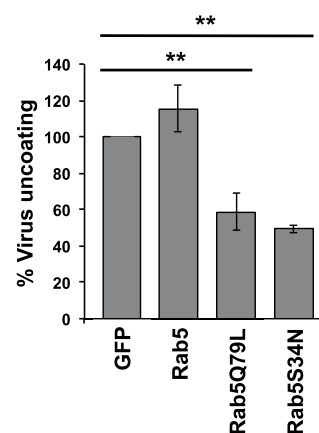
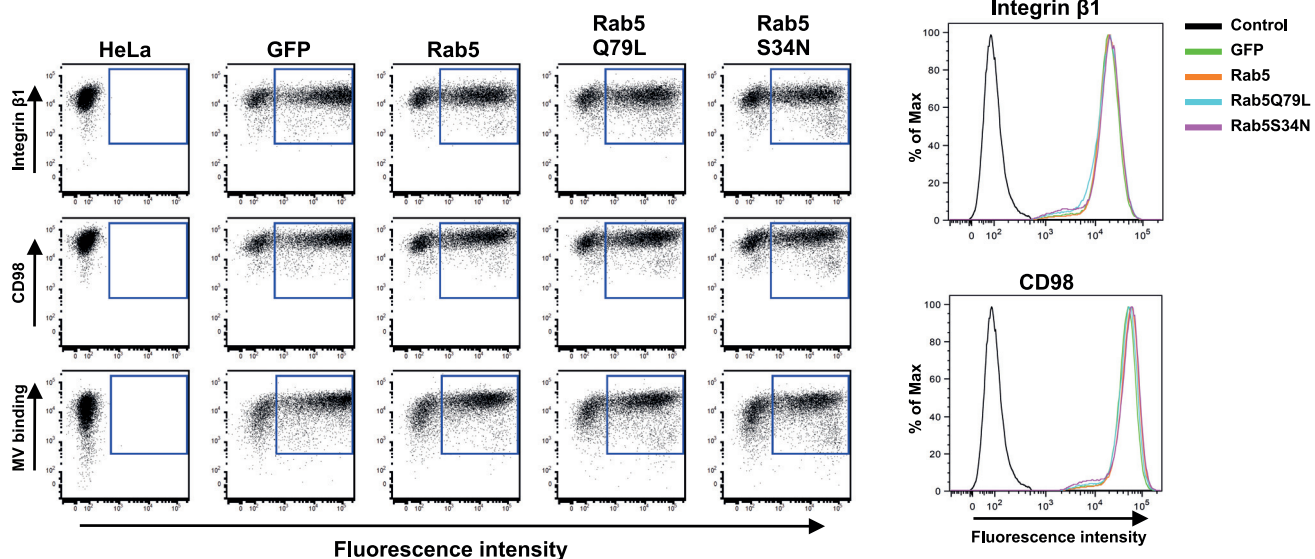
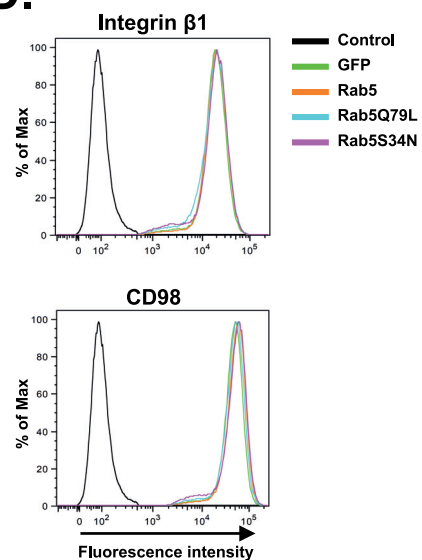
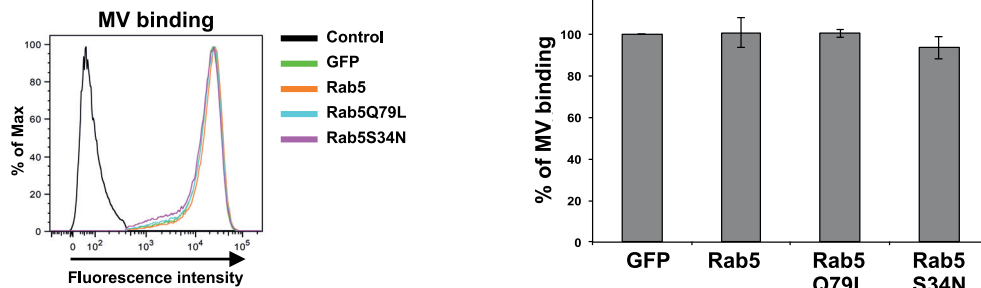
A.**B.****C.****D.****E.**

FIG 2 Vaccinia MV traffics through early endosomes prior to virus core uncoating. (A) HeLa cells were transfected with individual plasmids encoding GFP, GFP-Rab5, GFP-Rab5Q79L, and GFP-Rab5S34N and infected with wild-type (WT) WR MV for virus uncoating assays. The cells were stained with anti-A4 antibody, and cell images were collected using a confocal laser scanning microscope with a 63 \times objective lens. Green and white lines delineate the edges of GFP-expressing and non-GFP-expressing cells, respectively. The scale bar marks 20 μ m in length. (B) Quantification of the viral core uncoating assays of the cells in panel A. The number of A4 cores in each GFP-expressing cell were counted; the averaged numbers of viral cores per cell in GFP-expressing cells were considered to be 100%. Bars represent the standard deviations of three independent experiments. Statistical significance was determined using a Student *t* test. **, $P < 0.01$. (C) FACS analyses of the cell surface level of integrin β1, CD98, and surface-bound vaccinia MV in HeLa cells expressing GFP or GFP fused WT-Rab5, Rab5Q79L, and Rab5S34N protein. (D) Histogram of the cell surface levels of integrin β1 and CD98 in cells described in panel C. (E) Histogram and a bar chart showing mean fluorescence intensity (MFI) of cell surface-bound vaccinia MV in HeLa cells described in panel C.

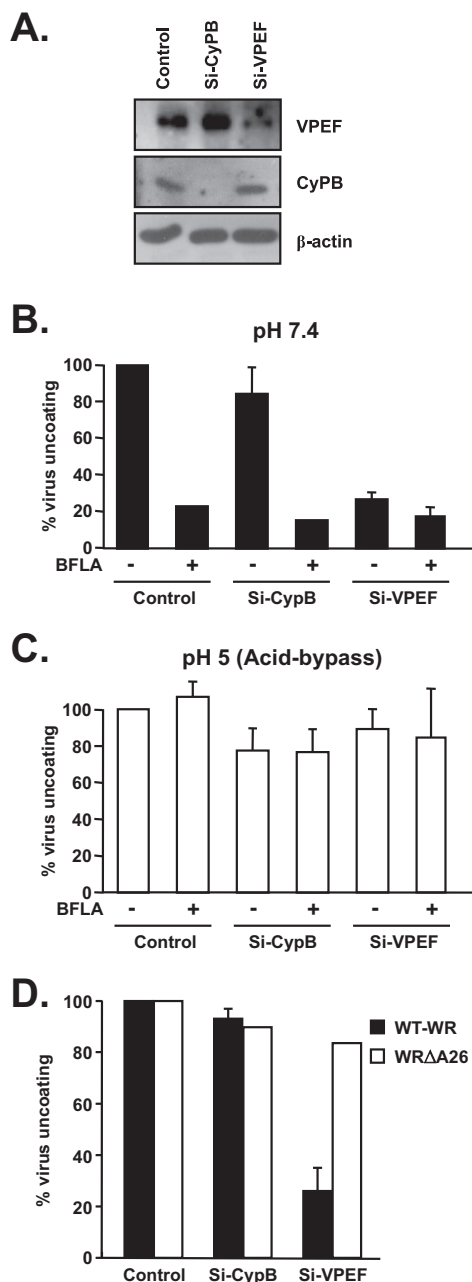


FIG 3 VPEF is specifically required for vaccinia MV entry via the endocytic route, not through plasma membrane fusion. (A) HeLa cells were either mock transfected (Control) or transfected with siRNA duplexes targeting CypB (Si-CypB) or VPEF (Si-VPEF) and then harvested for immunoblots with anti-VPEF, anti-CypB, and anti-β-actin antibodies. (B and C) The cells described in panel A were pretreated with DMSO (−) or 25 nM baflomycin A (BFLA) (+) and subsequently infected with WT-WR MV. The cells were treated for 3 min with either neutral buffer (pH 7.4) (B) or acidic buffer (pH 5) (C) and then used for virus uncoating assays. (D) The cells described in panel A were infected with WT-WR MV or WRΔA26 MV and used for virus uncoating assays. Bars represent the averages of two independent experiments.

formed experiments using the WRΔA26 virus, which enters HeLa cells through plasma membrane fusion at neutral pH (27, 39). If VPEF plays a specific role in virus endocytic route, we anticipated the protein to be dispensable for WRΔA26 virus entry. As ex-

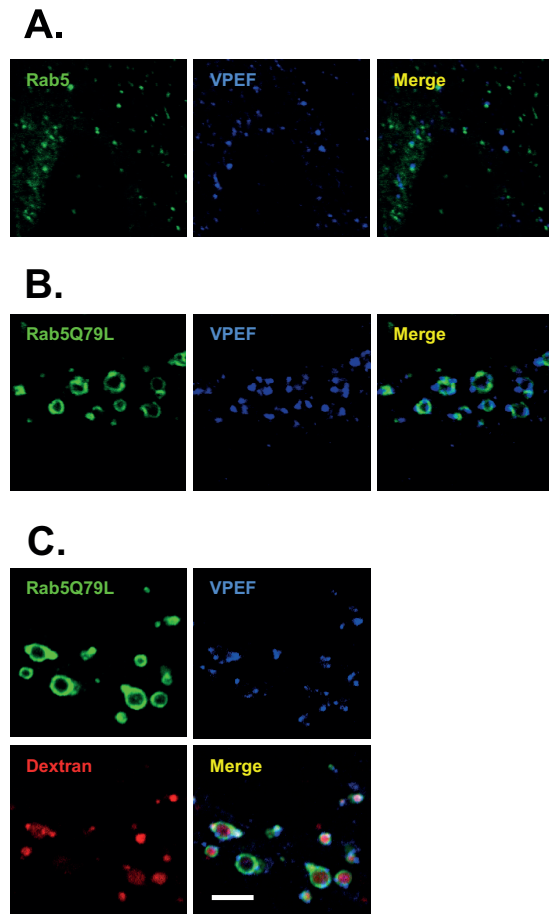


FIG 4 Dextran uptake is observed in VPEF-positive early endosomes in HeLa cells. (A and B) HeLa cells were transfected with plasmids expressing GFP-WT-Rab5 (A) or GFP-Rab5-Q79L (B). The cells were then stained with anti-VPEF antibodies for confocal microscopy analyses. (C) For dextran uptake, the HeLa cells expressing GFP-Rab5-Q79L from panel A were incubated with Texas Red-conjugated dextran, washed, and fixed. Cell images were collected using a confocal laser scanning microscope with a 40× objective lens. The scale bar marks 5 μm in length.

pected, VPEF knockdown in HeLa cells specifically reduced WT-WR MV, but not WRΔA26, entry into HeLa cells (Fig. 3D).

Our previous data showed that VPEF protein is predominantly distributed in cytoplasm as small speckles partially overlapping with Rab11 and Rab34, but not with Rab5 (20), suggesting that VPEF might be a vesicular protein that regulates vesicle trafficking. Gomez and Billadeau (37) and Derivery et al. (40) reported that VPEF (also called FAM21) is a component of the WASH protein complex that mediates branched actin polymerization and controls endosome membrane fission during cargo sorting out of early endosomes. Here, we transfected HeLa cells with wild-type Rab5-GFP and observed that only a small portion of VPEF staining colocalized with Rab5 (Fig. 4A). However, in HeLa cells transfected with GFP-Rab5-Q79L (which blocks endosome fission, resulting in enlarged endosomes), anti-VPEF antibody clearly stained “patches” of the enlarged endosome membranes, suggesting that VPEF was closely associated with endosome subdomains (Fig. 4B), in contrast to Rab5, which forms a ring around early endosomes. This is consistent with previous studies by Gomez and Billadeau (37). To examine whether these VPEF-containing enlarged endosomes accommodated extracellular li-

gand, we fed the cells with the fluorescent fluid phase marker dextran and observed dextran accumulation in VPEF-positive enlarged endosomes (Fig. 4C). These results confirmed that a portion of VPEF was associated with subdomains of early endosomes in HeLa cells.

The WASH protein complex contains several other proteins in addition to VPEF, including CapZ α 1, KIAA1033, KIAA0196, Hsp70 (A8 and 1A isoforms), and CCD53 (40). WASH recruits Arp2/3 and acts as a nucleation center for actin polymerization. VPEF forms a bridge between the WASH and CapZ α 1 proteins to regulate endosomal actin polymerization. The roles of other components in endosomal trafficking remain unknown (37, 40). To investigate this matter, we knocked down each of the above components of the WASH protein complex in HeLa cells (see Fig. S1 in the supplemental material), infected these cells with vaccinia WT-WR MV and WR Δ A26-MV, and performed virus core uncoating assays. We found that only three subcomponents of the WASH protein complex—VPEF, CapZ α 1, and WASH—were required for vaccinia WT-WR MV entry (Fig. 5A and B), while none of these components were required for WR Δ A26 virus entry (see Fig. S2 in the supplemental material). These findings suggested that CapZ α 1-VPEF-WASH facilitates virus entry by regulating actin polymerization for endosomal sorting.

Furthermore, we overexpressed a GFP fusion protein, including the N-terminal region of VPEF (amino acids 1 to 356), which is the WASH-binding domain. This protein, designated GFP-VPEF(aa1-356), functions as a dominant-negative protein that interferes with the trafficking of cellular receptors, such as the mannose-6-phosphate receptor (M6PR) (37). Figure 5C shows that GFP-VPEF(aa1-356) overexpression interfered with M6PR trafficking from early endosomes to Golgi. More importantly, GFP-VPEF(aa1-356) overexpression reduced WT-WR MV core uncoating (Fig. 5D and E), demonstrating the importance of WASH in WT-WR MV entry. Altogether, our results showed that the association between VPEF and WASH to mediate actin polymerization is critical for endosomal fission and, consequently, for the further sorting of vaccinia MV-containing vesicles.

Retromer complexes associated with VPEF are also required for early endosomal sorting of WR-MV. The C-terminal region of VPEF binds to Vps35, a retromer complex component that mediates both endosome-to-Golgi and endosome-to-plasma-membrane endosomal protein sorting (41). Retromers include two subcomplexes: Vps26-29-35 and sorting nexin 1 (SNX1-SNX1) dimers (42). Lacking a suitable anti-Vps26 antibody for immunofluorescence studies, we transfected Vps26-GFP into HeLa cells. Vps26 colocalized with Vps35, as expected, and it also colocalized with VPEF on early endosomes (Fig. 6A). Furthermore, endogenous WASH partially colocalized with Vps35 and SNX1 on early endosomes (Fig. 6B), confirming that the WASH protein complex associates with retromers on early endosomes.

We next addressed whether WASH-associated retromers were important for WR-MV entry. We knocked down CypB (control), WASH, or three retromer components—SNX1, Vps35 (Fig. 6C), and Vps26 (Fig. 6E)—in HeLa cells and infected these cells with WT-WR or WR Δ A26 virus for core uncoating assays (Fig. 6D and F). The results showed that retromers were important for WT-WR endocytic trafficking but not for WR Δ A26 virus cell entry, confirming that retromer protein machinery plays a specific role in governing WT-WR MV sorting.

Vaccinia WT-WR traffics through Rab11-positive and Rab22-positive recycling endosomes prior to viral core uncoating in cytoplasm. During trafficking through early endosomes,

internalized cellular receptor cargos could either be transported to Rab7-positive late endosomes/lysosomes for degradation or to Rab11-containing recycling endosomes that may either be recycled back to the plasma membrane or further transported to the Golgi apparatus (43, 44). Cargos such as integrin β 1 can be recycled through Rab11 regulated-recycling endosomes that directly transport cargo from endosomes to either the Golgi membrane or back to the plasma membrane (45–47). Knowing that WT-WR MV binds integrin β 1 during entry, we rationalized that virus-receptor interaction may dictate subsequent intracellular trafficking specificity. Moreover, a fraction of intracellular VPEF protein staining colocalizes with Rab11 (20). Thus, we next imaged single virus particle association with Rab11-positive recycling endosomes in HeLa cells, similar to our above-described examination of the WT-WR MV association with Rab5-positive early endosomes.

As shown in Fig. 7, we observed colocalization of fluorescent vaccinia MV particles with wild-type GFP-Rab11 (Fig. 7A and B; see also Movie S3 in the supplemental material). Tracking of 155 single virus particles showed that ~8.0% of vaccinia MV particles were colocalized with Rab11-positive recycling endosomes early after infection, whereas this proportion increased to ~27% during the late second phase (Fig. 7C). 3D triple-color time-lapse tracking was also performed and an example of MV endocytic trafficking itinerary showed that a virus particle colocalized with a Rab5-positive endosome at 42 min postinfection and merged with a Rab11-positive recycling endosome at 50 to 55 min postinfection, as shown by the colocalization of CFP-MV, mCherry-Rab5, and GFP-Rab11 (Fig. 7D). The 3D trajectory of this virus colocalization with Rab5 and Rab11 is shown in Movie S4 in the supplemental material. We next transfected HeLa cells with GFP alone, GFP-Rab11, GFP-Rab11Q70L, and GFP-Rab11S25N and infected these cells with WT-WR MV for virus uncoating assays. Wild-type GFP or GFP-Rab11 expression did not affect virus uncoating. However, the expression of GFP-Rab11Q70L and GFP-Rab11S25N significantly reduced the release of viral cores into cytoplasm (Fig. 7E and F). As control experiments, we also confirmed that the cell surface levels of integrin β 1 and CD98 molecules (Fig. 7G and H), as well as the amount of vaccinia MV binding (Fig. 7I) on HeLa cells overexpressing wild-type GFP alone, GFP-Rab11, Rab11Q70L, and GFP-Rab11S25N, were not reduced. Overall, these results supported that internalized vaccinia WT-WR MV trafficked through Rab11-positive recycling endosomes prior to membrane fusion and viral core release in the cytoplasm.

It has also been reported that surface protein CD98 is internalized to early endosomes and subsequently recycled through specific Rab22-positive recycling tubules (48). We previously showed that CD98 is specifically required for vaccinia WT-WR MV endocytosis and not for plasma membrane fusion (19); thus, we tested whether vaccinia MV may traffic through the Rab22-mediated recycling pathway. HeLa cells were transfected with wild-type GFP-Rab22 and infected with WR-A4-mCherry for single particle tracking (Fig. 8A; see Movie S5 in the supplemental material) and trajectory tracing analyses (Fig. 8B). Similar to Rab11 association with MV, we observed Rab22 association with MV at both early and late phase, with an increase of 2-fold colocalization in the late phase (~36% for late versus 16% for early phase) (Fig. 8C). 3D triple-color time-lapse tracking analyses were performed and provided further evidence to confirm this possibility. A typical example of MV endocytic trafficking itinerary showed that this partic-

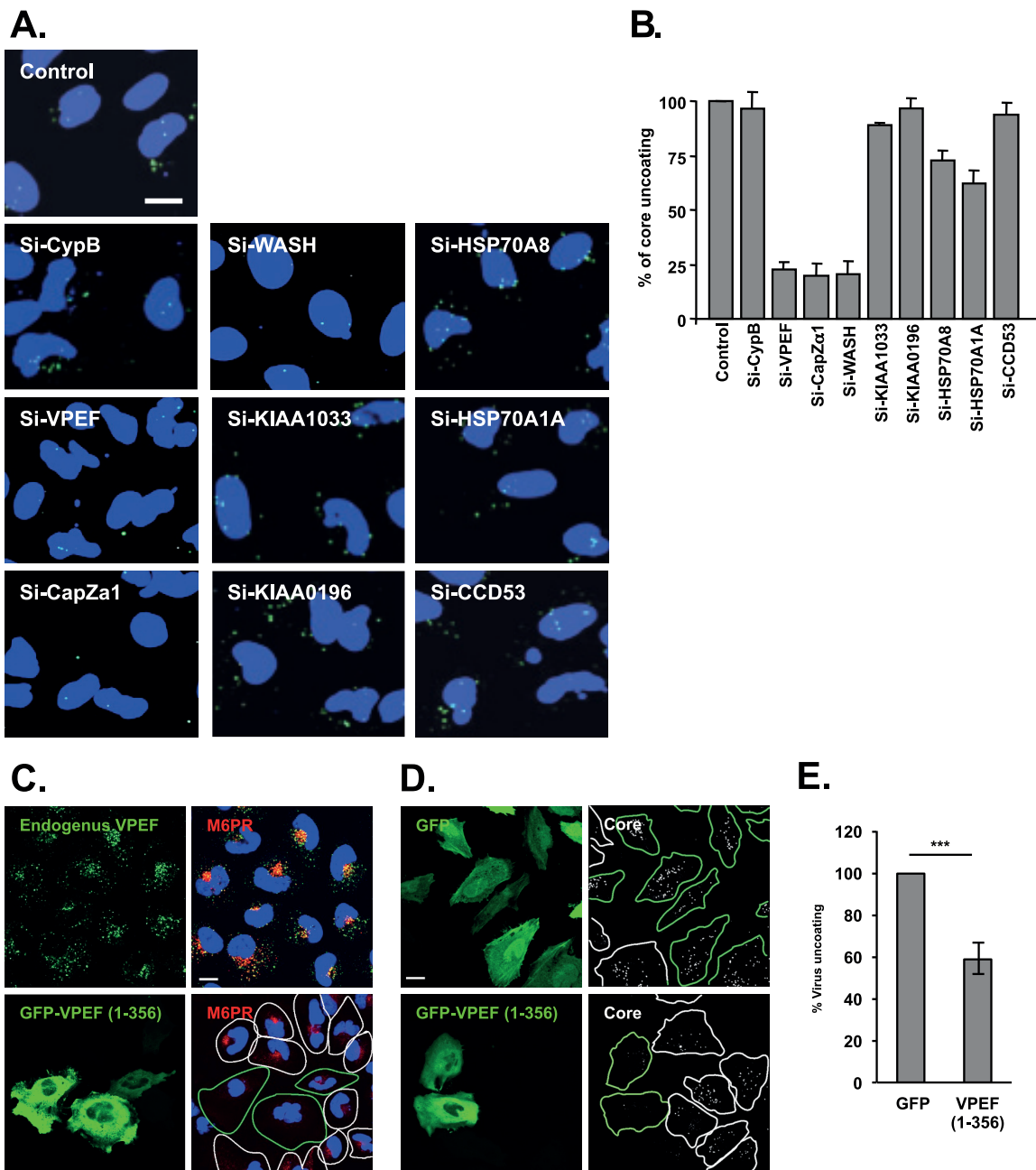


FIG 5 VPEF-associated WASH and CapZ α 1 proteins are required for vaccinia MV endocytosis. (A) Knocking down WASH and CapZ α 1 in HeLa cells also reduced virus core uncoating. HeLa cells were either mock transfected (Control) or transfected with siRNA duplexes targeting CypB (Si-CypB), VPEF (Si-VPEF), CapZ α 1 (Si-CapZ α 1), WASH (Si-WASH), KIAA1033 (Si-KIAA1033), KIAA0196 (Si-KIAA0196), HSP70A8 (Si-HSP70A8), HSP70A1A (Si-HSP70A1A), or CCD53 (Si-CCD53) and subsequently infected with WT-WR MV for virus uncoating assays. The knockdown efficiency of each gene is shown in Fig. S1 in the supplemental material. Cell viral cores were stained with anti-A4 antibody (green) and analyzed by confocal laser scanning microscope with a 40 \times objective lens. (B) Quantification of viral core uncoating in the knockdown cells shown in panel A. The averaged viral core numbers in control HeLa cells were considered to be 100%. The experiments were repeated twice, and the averages are shown. (C) GFP-VPEF(aa1-356) overexpression in HeLa cells inhibited M6PR intracellular trafficking. HeLa cells were mock transfected (top panels) or transfected with a plasmid expressing GFP-VPEF(aa1-356) (bottom panels), incubated with anti-Cl-MPR antibody to trigger M6PR internalization, and then stained with rhodamine anti-mouse monoclonal antibody (red), anti-VPEF antibody plus fluorescein isothiocyanate (FITC)-conjugated anti-rabbit antibody (green, in top panel only), and nuclear DNA for confocal microscopy analyses. Green and white lines delineate the edges of GFP-expressing or non-GFP-expressing cells, respectively. (D) GFP-VPEF(aa1-356) overexpression in HeLa cells inhibited WT-WR MV core uncoating. HeLa cells were transfected with GFP and GFP-VPEF(aa1-356) and infected with WT-WR MV for virus core uncoating assays. Green and white lines delineate the edges of GFP-expressing or non-GFP-expressing cells, respectively. (E) Quantification of virus uncoating assays of cells in panel D. The averaged numbers of viral cores per cell in GFP-expressing cells were considered to be 100%. The experiments were repeated three times. Statistical significance was determined by using a Student *t* test. ***, *P* < 0.001. The white scale bar in the images represents 20 μ m in length.

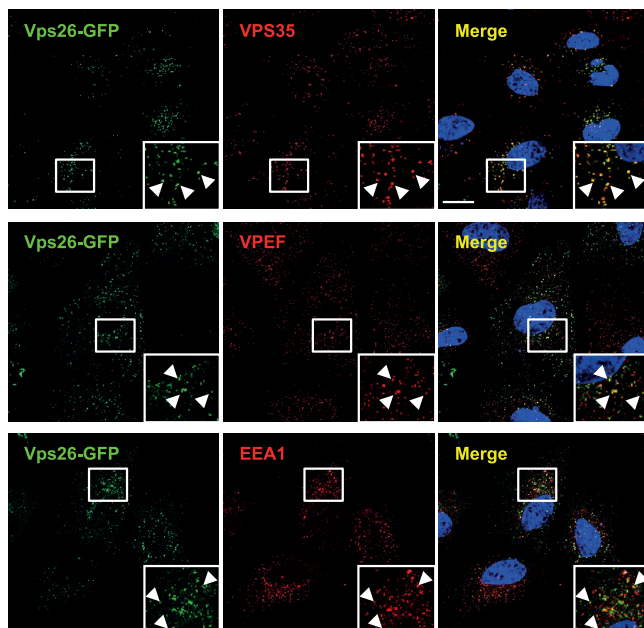
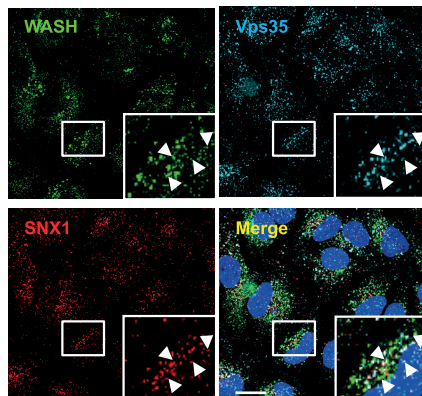
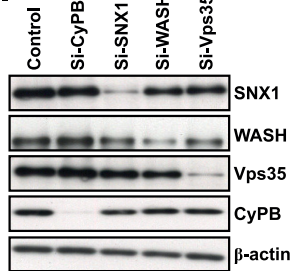
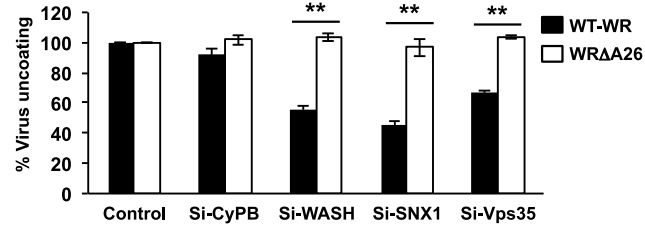
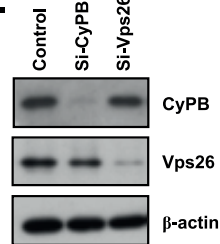
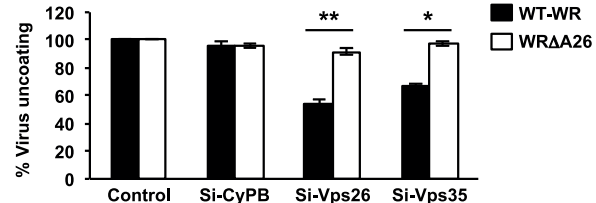
A.**B.****C.****D.****E.****F.**

FIG 6 Retromers are specifically required for endocytic entry of vaccinia WT-WR MV but not for WRΔA26 MV that enters HeLa cells through plasma membrane fusion. (A) VPEF was associated with retromers on early endosomes. HeLa cells were transfected with a plasmid expressing GFP-VPS26 and then stained with anti-VPS35, anti-VPEF, and anti-EEA1 antibodies. The insets show good colocalization (marked by white arrowheads) of GFP-VPS26 with endogenous VPS35, VPEF, and EEA1, respectively. (B) WASH protein colocalized with retromers in HeLa cells. HeLa cells were stained with anti-WASH (green), anti-Vps35 (cyan), and anti-SNX1 (red) antibodies. The insets show good colocalization (marked by white arrowheads) among endogenous WASH, Vps35, and SNX1 proteins. (C to F) Knockdown of the retromer components Vps35, Vps26, and SNX1 reduced WT-MV endocytosis but not WRΔA26 MV plasma membrane fusion. HeLa cells were either mock transfected (Control) or transfected with siRNA duplexes targeting CypB (Si-CypB), SNX1 (Si-SNX1), WASH (Si-WASH), or Vps35 (Si-Vps35) (in panels C and D) or Vps26 (in panels E and F). These cells were then subjected to immunoblot analyses (in panels C and E) or infected with WT-WR MV or WRΔA26 MV for virus uncoating assays (in panels D and F). The core numbers obtained in control HeLa cells were considered to be 100%. The bars represent the standard deviations of three independent experiments. Statistical significance was determined by using a Student *t* test. *, *P* < 0.05; **, *P* < 0.01. The white scale bar in the images represents 20 μm in length.

ular virus particle colocalized with a Rab5-positive endosome at 44 min postinfection and merged with a Rab22-positive recycling endosome at 49 min postinfection, as shown by the colocalization of CFP-MV, mCherry-Rab5, and GFP-Rab22 (Fig. 8D). The 3D

trajectory is shown in Movie S6 in the supplemental material. We then analyzed virus core uncoating in HeLa cells transfected with wild-type GFP alone, GFP-Rab22, GFP-Rab22Q64L, and GFP-Rab22S19N (Fig. 8E and F). Inhibition of virus core uncoating was

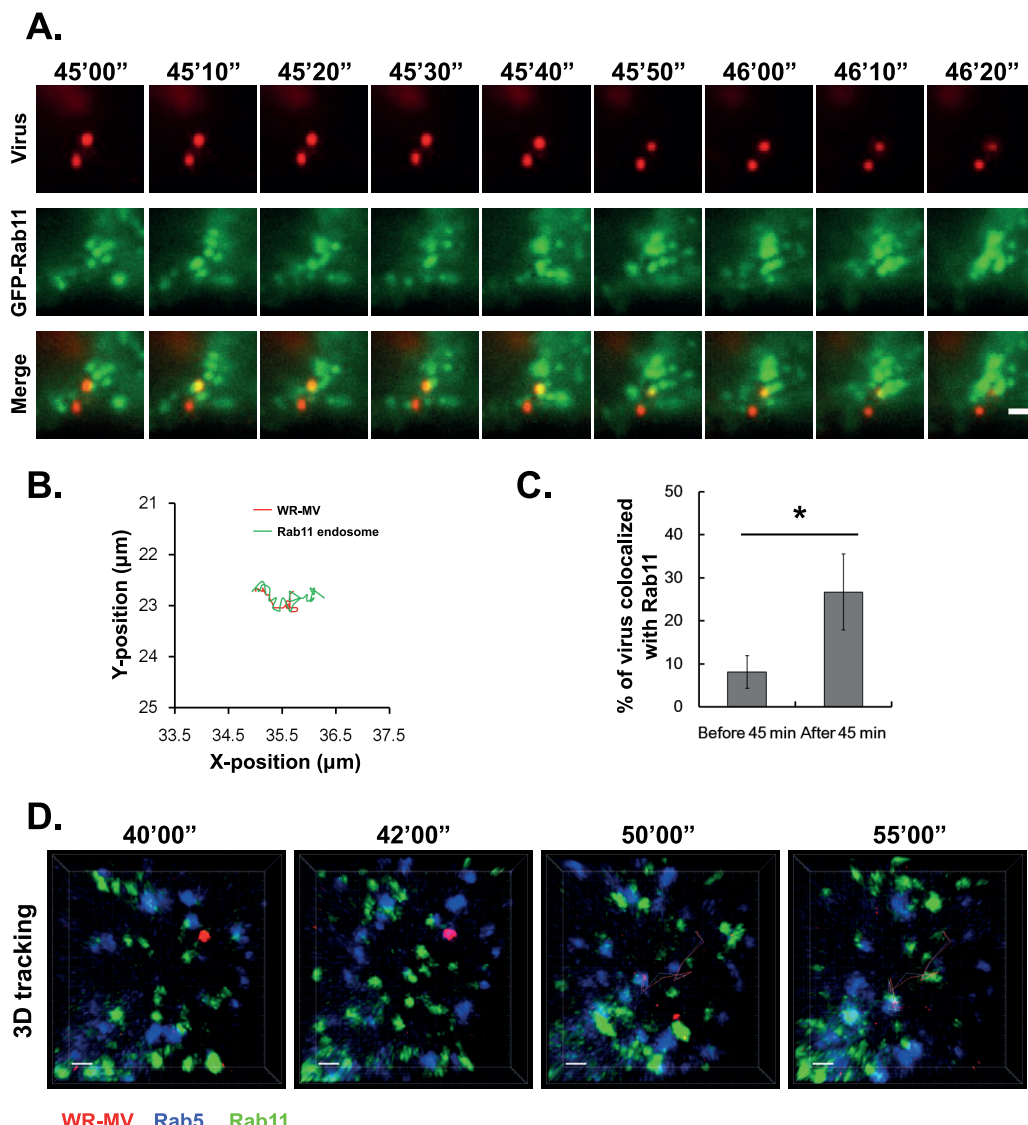


FIG 7 Vaccinia MV traffics through Rab11-positive recycling endosomes. (A) The represented frames show the endocytic trafficking behavior of a single fluorescent vaccinia WR-A4-mCherry MV particle colocalized with the GFP-Rab11 recycling endosome. A4-mCherry MV particles, red (top panel); GFP-Rab11 recycling endosomes, green (middle panel); vesicles containing both A4-mCherry MV particle and GFP-Rab11, a marker of recycling endosomes, yellow (bottom panel). The scale bar represents 1 μm in length. (B) The overlapped trajectory profiles of a A4-mCherry MV particle (red) and a GFP-Rab11 recycling endosome (green) in a HeLa cell. (C) Histogram showing A4-mCherry MV particles colocalized with Rab11-positive endosomes. A total of 155 viral particles were tracked. The data were from three independent replicates. Statistical significance was determined by using a Student *t* test. *, $P < 0.05$. (D) Cotrafficking of a A4-CFP MV particle (in red) with mCherry-rab5 (in blue) and GFP-Rab11-positive (in green) endosome revealed by 3D time-lapse tracking using a spinning disk confocal microscopy. The selected time frames showed the 3D trafficking behavior of single A4-CFP MV particle with Rab5-positive and Rab11-positive endosomes in a cell and the 3D trajectory of virus particle trafficking is shown in Movie S4 in the supplemental material. The scale bar represents 1 μm . (E) HeLa cells were transfected with individual plasmids encoding GFP, GFP-Rab11, GFP-Rab11Q70L, and GFP-Rab11S25N and infected with WT-WR MV for virus uncoating assays. Cells were stained with anti-A4 antibody, and cell images were collected by confocal laser scanning microscope using a 63 \times objective lens. The scale bar represents 20 μm in length. Green and white lines delineate the edges of GFP-expressing or non-GFP-expressing cells, respectively. (F) Quantification of the viral core uncoating assays of the cells in panel E. The numbers of A4 cores in each GFP-Rab11-expressing cell were counted and normalized to the numbers of A4 cores in GFP-expressing cells. The bars represent the standard deviations of three independent experiments. Statistical significance was determined by using a Student *t* test. **, $P < 0.01$. (G) FACS analyses of the cell surface levels of integrin $\beta 1$, CD98, and surface-bound vaccinia MV in HeLa cells expressing GFP, GFP-WT-Rab11, GFP-Rab11Q70L and Rab11S25N protein, respectively, were conducted. (H) Histograms of cell surface level of integrin $\beta 1$ and CD98 in cells described in panel G. (I) Histogram (left panel) and quantification data (right panel) of cell surface-bound vaccinia MV in HeLa cells described in panel G.

observed in HeLa cells expressing GFP-Rab22Q64L and GFP-Rab22S19N, but not wt-GFP-Rab22 or GFP. As control experiments, we also confirmed that the cell surface levels of integrin $\beta 1$ and CD98 molecules (Fig. 8G and H), as well as the amount of vaccinia MV binding (Fig. 8I), were not reduced in cells expressing

GFP, wild-type Rab22, or Rab22Q64L proteins. Interestingly, we noticed a small reduction of surface receptor integrin $\beta 1$ level (~15%) and MV binding (~14%) in cells expressing Rab22S19N. Although 14% reduction of MV binding was not statistically significant and did not account for the 60% reduction of virus un-

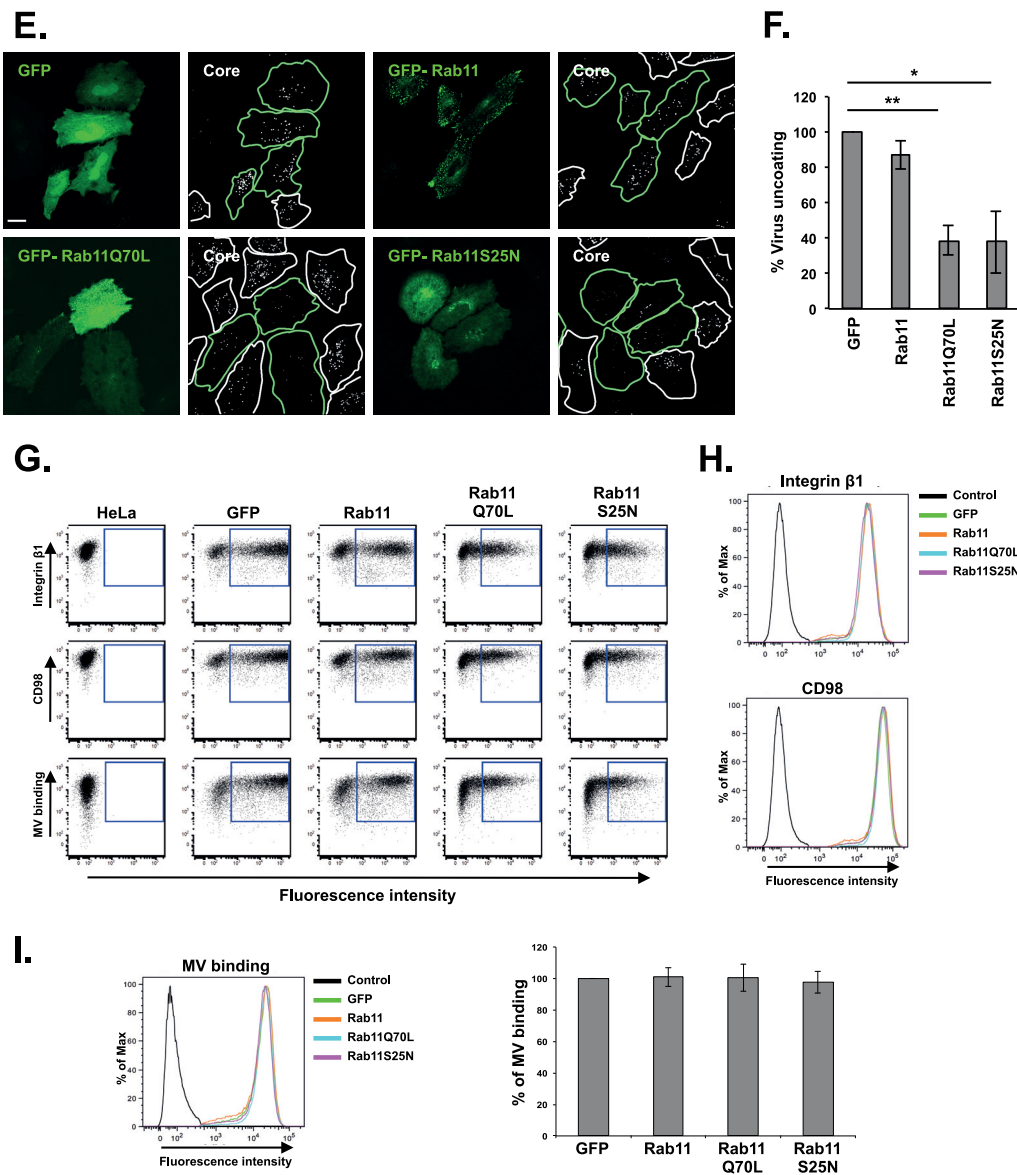


FIG 7 continued

coating in cells (Fig. 8F), it remains an interesting possibility that Rab22 may regulate MV entry through multiple mechanisms, such as surface receptor integrin $\beta 1$ recycling, MV attachment to cells, and virus trafficking in cells. Altogether, our results showed both Rab11 and Rab22 participated in endosomal trafficking of vaccinia WT-MV prior to core uncoating.

Finally, we performed imaging analyses to monitor the association between WT-WR MV and Rab7-positive late endosome/lysosomes. We observed very little WT-WR MV colocalization with Rab7-positive late endosome/lysosomes (Fig. 9A; see also Movie S7 in the supplemental material). Furthermore, even a low level ($\sim 5\%$) of colocalization was observed throughout the 90-min infection period, this colocalization did not appear to be kinetically regulated, implying a possible stochastic association (Fig. 9B). We then transfected wild-type CFP alone, CFP-Rab7, CFP-Rab7Q67L, and CFP-Rab7T22N into HeLa cells (Fig. 9C), and we detected no significant inhibition of virus core uncoating in

all cases, demonstrating that WR-MV did not traffic to the late endosome/lysosome for virus uncoating (Fig. 9D). Again, cell surface levels of integrin $\beta 1$ and CD98 molecules, as well as the amount of vaccinia MV binding on HeLa cells, were not reduced by any of the CFP-Rab11 fusion proteins described above (Fig. 9E to G).

Rab34 reportedly plays a role in a clathrin-independent, caveola-independent cargo transport pathway. It was also shown that Rab34 participates in fluid-phase uptake by promoting macropinosome formation (49), although another report demonstrated that dextran uptake and trafficking was independent from Rab34 function (50). Rab34 also functions in cellular secretory pathway and mediates vesicular stomatitis virus (VSV) G protein trafficking from Golgi to plasma membrane (50). To investigate whether Rab34 was involved in vaccinia WT-WR MV entry, HeLa cells were transfected with GFP alone, GFP-Rab34, GFP-Rab34Q111L, and GFP-Rab34T66N and infected with vaccinia WT-MV for a virus uncoating assay

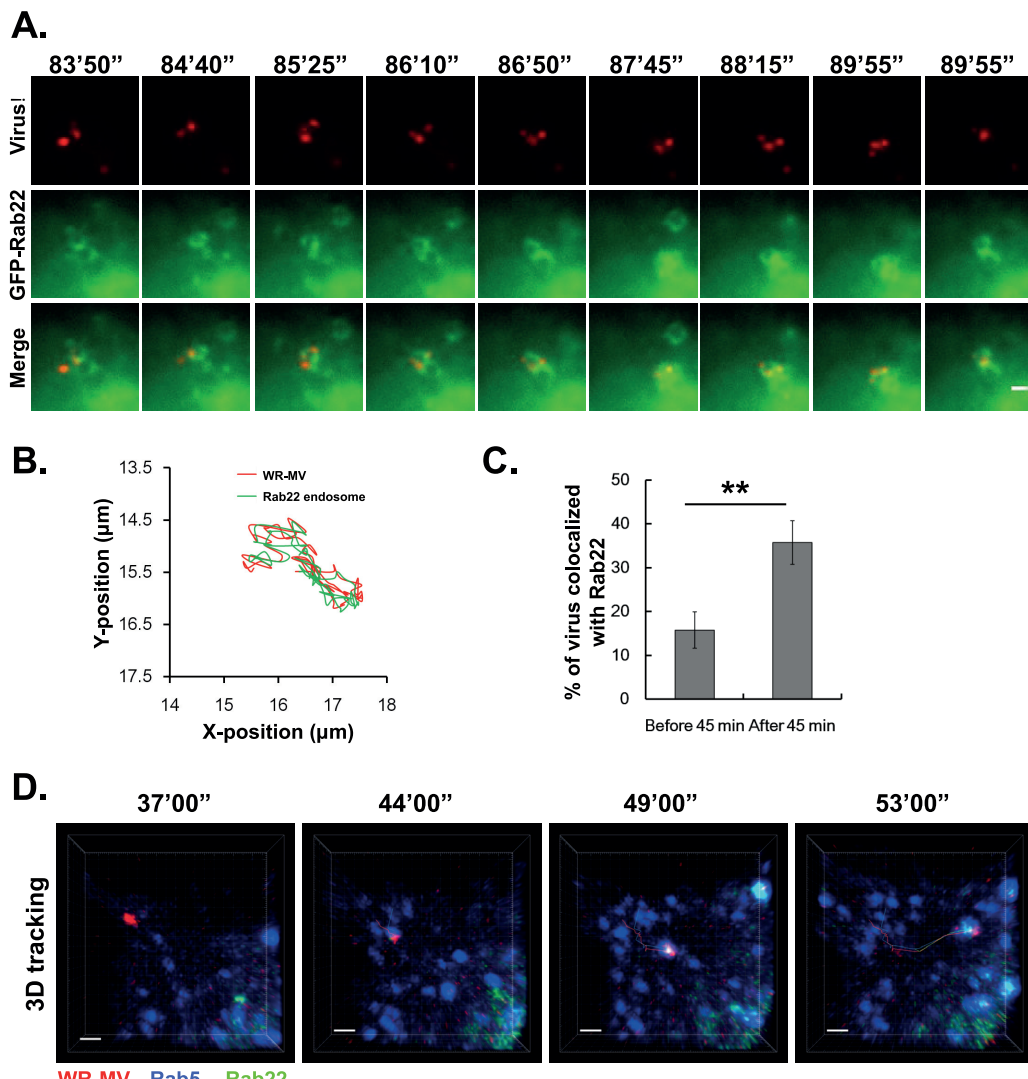


FIG 8 Vaccinia MV traffics through Rab22-positive recycling endosomes. (A) The selected frames show the endocytic trafficking behavior of a single fluorescent vaccinia WR-A4-mCherry MV particle colocalized with a GFP-Rab22 recycling endosome. A4-mCherry MV particles, red (top panel); GFP-Rab22 recycling endosomes, green (middle panel); vesicles containing both A4-mCherry MV particle and GFP-Rab22 recycling endosome, yellow (bottom panel). The scale bar represents 1 μm in length. (B) Overlapped trajectory profiles of a A4-mCherry MV particle (red) and a GFP-Rab22 recycling endosome (green) in a HeLa cell. (C) Histogram of A4-mCherry MV particles colocalized with Rab22-positive endosomes. A total of 169 viral particles were tracked. The data are from three independent replicates. Statistical significance was determined by using a Student *t* test. **, $P < 0.01$. (D) Selected frames from a representative time series of 3D tracking showing a sequential colocalization of vaccinia A4-CFP MV particles (red) with mCherry-Rab5 (blue) and GFP-Rab22 (green) in a cell using a spinning disk confocal microscopy. The 3D trajectory of virus particle cotrafficking is shown in Movie S6 in the supplemental material. The scale bar represents 1 μm in length. (E) Expression of Rab22 mutant proteins inhibited vaccinia MV entry. HeLa cells were transfected with individual plasmids encoding GFP, GFP-Rab22, GFP-Rab22Q64L, and GFP-Rab22S19N and infected with WT-WR MV for virus uncoating assays. Cells were then stained with anti-A4 antibody, and images were collected by confocal laser scanning microscope by using a 63 \times objective lens. Green and white lines delineate the edges of GFP-expressing or non-GFP-expressing cells, respectively. The scale bar represents 20 μm in length. (F) Quantification of the viral core uncoating assays of the cells in panel E. The numbers of A4 cores in each GFP-Rab22-expressing cell were counted and normalized to the numbers of A4 cores in GFP-expressing cells. After normalization, the core number in GFP expressing cells was considered to be 100% virus core uncoating. The bars represent the standard deviations of three independent experiments. Statistical significance was determined by using a Student *t* test. **, $P < 0.01$. (G) FACS analyses of cell surface levels of integrin $\beta 1$, CD98, and surface-bound vaccinia MV in HeLa cells expressing GFP or GFP-fused WT-Rab22, RabQ64L, and Rab22S19N proteins. (H) Histogram showing cell surface expression of integrin $\beta 1$ and CD98 in HeLa cells expressing different Rab22 proteins as described in panel G. (I) Histogram (left panel) and quantification (right panel) showing the levels of cell surface-bound vaccinia MV on HeLa cells expressing different Rab22 proteins as described in panel G.

(see Fig. S3 in the supplemental material). Immunofluorescence and quantification data revealed no obvious inhibition of vaccinia WT-WR MV uncoating in these cells, suggesting that vaccinia MV entry through fluid-phase endocytosis was Rab34 independent.

DISCUSSION

Vaccinia MV enters cells through either endocytosis or plasma membrane fusion, depending on the involved virus strain (6, 8–10, 51) and the cell type (7, 22, 52–54). We previously showed that vaccinia MV of the WR strain enters HeLa and MEF cells

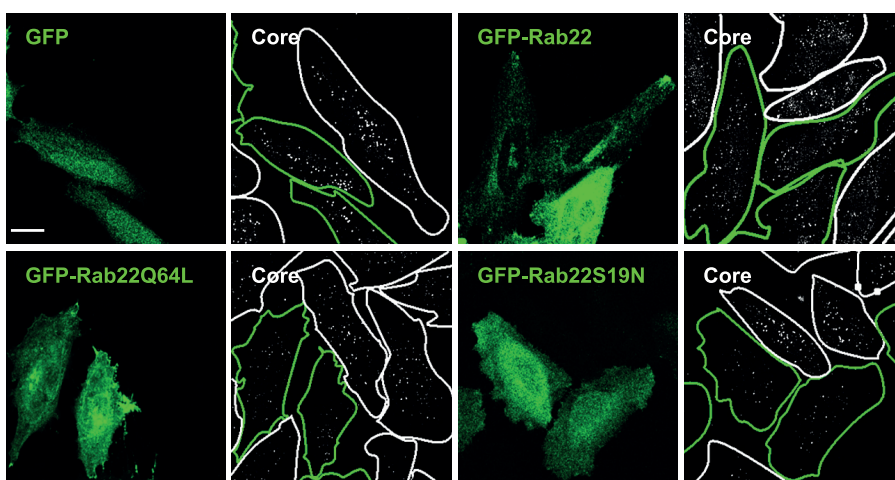
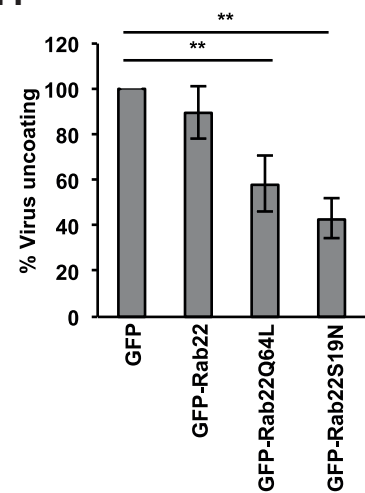
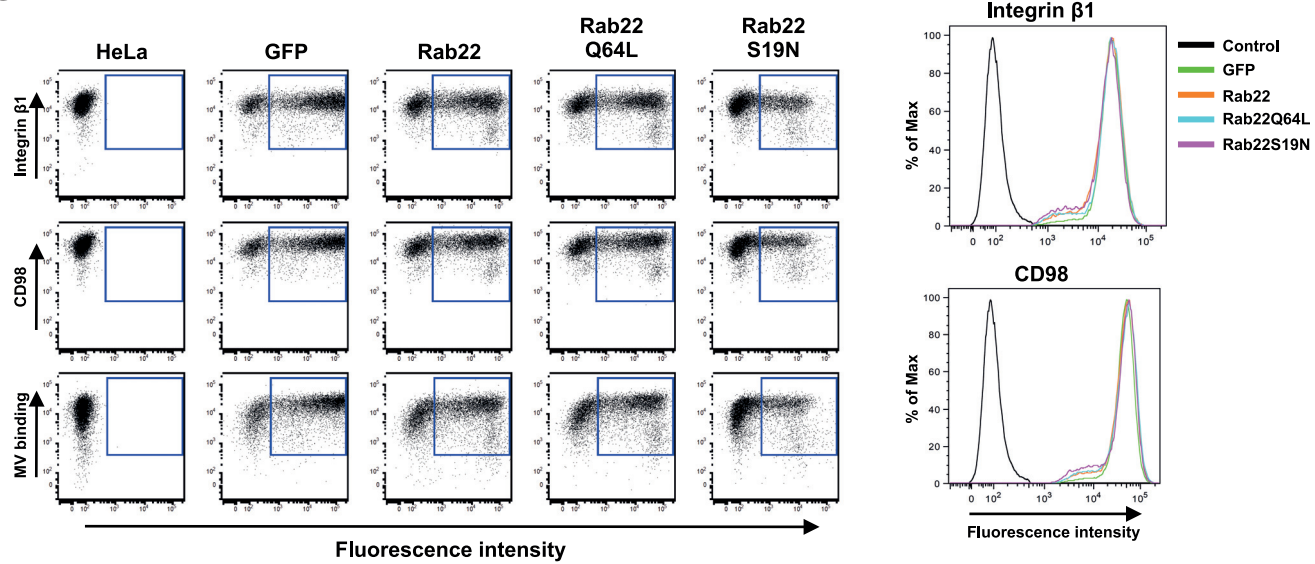
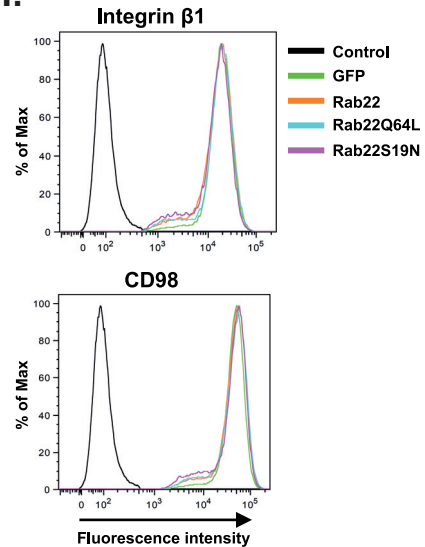
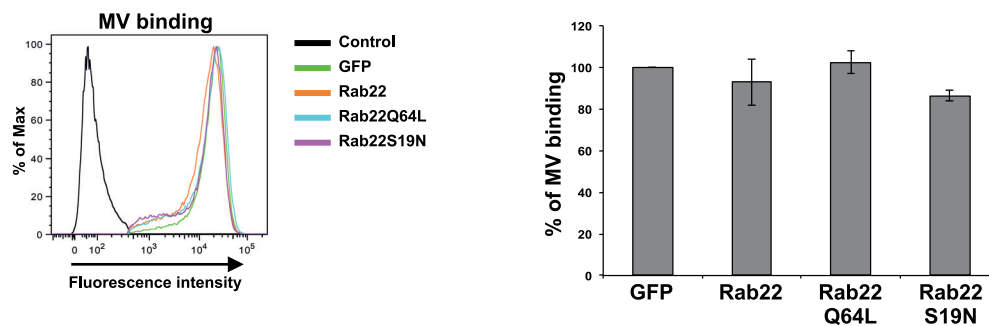
E.**F.****G.****H.****I.**

FIG 8 continued

through fluid-phase endocytosis, after which the internalized MV particles associate with PI3P-positive macropinosomes and Rab5-positive endosomes (19, 20). However, the subsequent intracellular trafficking pathway of MV was not investigated. In the present study, we further investigated the intracellular trafficking of WT-MV prior to viral core uncoating in the cytoplasm.

During the transportation of cellular cargos that target to different vesicles, Rab5 is localized to early endosome and Rab7 is localized to late endosome/lysosome, and both regulate receptor cargo trafficking from endosomes to late endosome/lysosomes for protein degradation. Alternatively, receptor cargo can traffic through a recycling pathway that directs cargo transport from

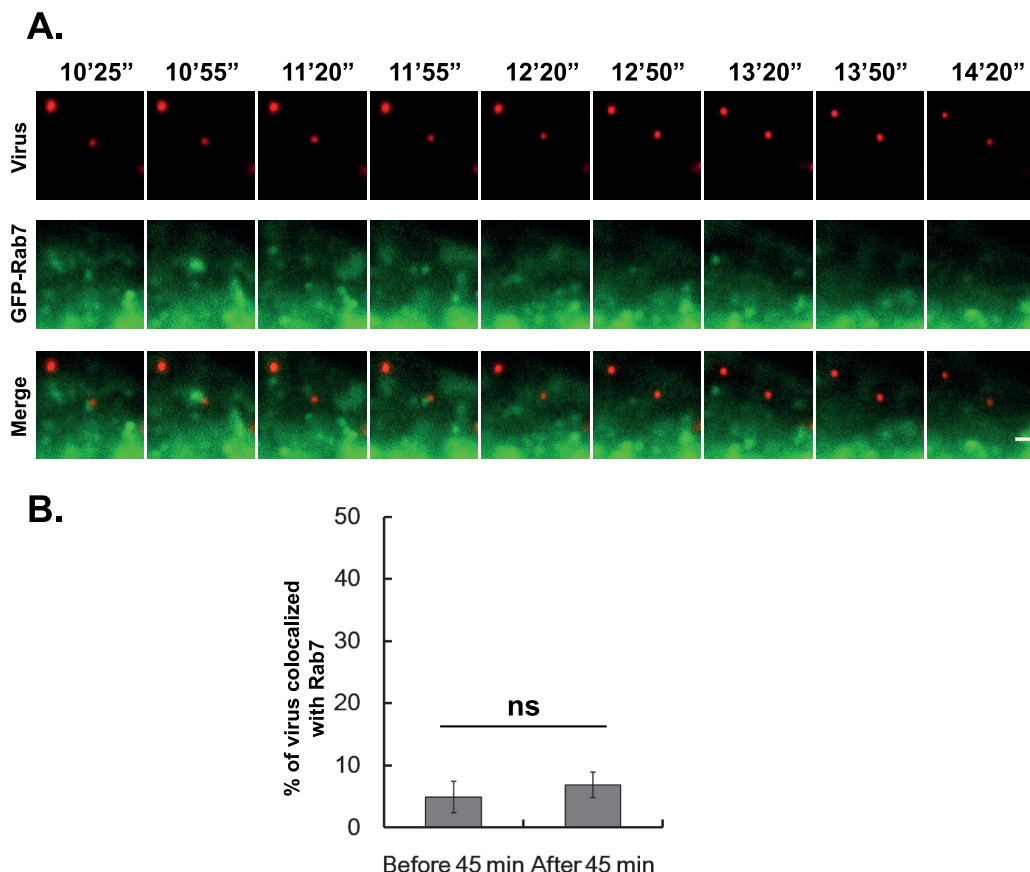


FIG 9 Vaccinia virus does not go through Rab7-positive late endosomes/lysosomes. (A) Selected frames show the endocytic trafficking behaviors of fluorescent vaccinia WR-A4-mCherry MV particles and CFP-Rab7 late endosomes. A4-mCherry MV particles, red (top panel); CFP-Rab7 late endosomes, green (middle panel). There was no obvious colocalization in the merged image of A4-mCherry MV particle and CFP-Rab7-positive endosomes (bottom panel). The scale bar represents 1 μ m in length. (B) Histogram showing A4-mCherry MV particles colocalized with CFP-Rab7-positive endosomes. A total of 277 particles were tracked. The data are from three independent replicates. Statistical significance was determined by using a Student *t* test. ns, nonsignificant. (C) HeLa cells were transfected with individual plasmids encoding CFP, CFP-Rab7, CFP-Rab7Q67L, and CFP-Rab7T22N and infected with WT-WR for virus uncoating assays. The cells were stained with anti-A4 antibody, and cell images were collected by confocal laser scanning microscope using a 63 \times objective lens. Cyan and white lines delineate the edges of CFP-expressing or non-GFP-expressing cells, respectively. The scale bar represents 20 μ m in length. (D) Quantification of the viral core uncoating assays of the cells in panel C. The numbers of A4 cores in CFP-expressing cell were counted and used as 100% to normalize the numbers of A4 cores in CFP-Rab7 expressing cells. The bars represent the standard deviations of three independent experiments. No statistical differences were found among these data sets. (E) FACS analyses of cell surface levels of integrin β 1, CD98, and surface-bound vaccinia MV in HeLa cells expressing GFP or CFP-WT-Rab7, CFP-Rab7Q67L, and CFP-Rab7T22N proteins. (F) Histograms of cell surface level of integrin β 1 and CD98 in cells described in panel E. (G) Histogram (left panel) and quantification data showing the mean fluorescence intensity (MFI) of cell surface-bound vaccinia MV (right panel) in the HeLa cells described in panel E.

endosomes either toward the Golgi or back to the plasma membrane. We tracked single virus particle movement along with fluorescence-labeled small GTPase proteins in cells using two methods: (i) conventional wide-field immunofluorescence microscopy that provides large numbers of virus entry events for quantification analyses and (ii) spinning disc confocal microscopy that allows us to track each viruses with better resolution and high specificity. To exclude the possibility of stochastic WT-WR MV colocalization with vesicles, we also constitutively expressed GTP-bound or GDP-bound forms of Rab mutant proteins to interfere with endogenous Rab protein function. Together, our data suggested that endocytosed vaccinia MV trafficked to Rab5-positive early endosomes and was further associated with Rab11-positive and Rab22-positive recycling endosome compartments prior to membrane fusion and virus uncoating in the cytoplasm (Fig. 10). It is worth pointing out that although Rab11 and Rab22 seemed to

interact more with MV containing vesicles after 45 min of virus infection, early interactions between Rab11 and Rab22 with MV-containing vesicles also existed. Since Rab22S19N expression in cells resulted in a moderate reduction of surface integrin β 1 level (\sim 15%) and MV binding (\sim 14%) (Fig. 8H and I), it may imply an interesting possibility that small GTPases such as Rab22 may affect MV entry through multiple mechanisms such as surface receptor integrin β 1 recycling, MV attachment to cells, and virus trafficking in cells (Fig. 10). Although it was also reported that Rab22 regulates recycling of CD98 from cell surface, we did not observe any reduction of CD98 level on plasma membrane in cells expressing Rab22S19N nor Rab22 Q64L. It could be that CD98 was a stable membrane protein on HeLa cells so the surface protein level was not significantly affected even when recycling pathway in cells was temporarily inhibited by expression of Rab22 mutant proteins.

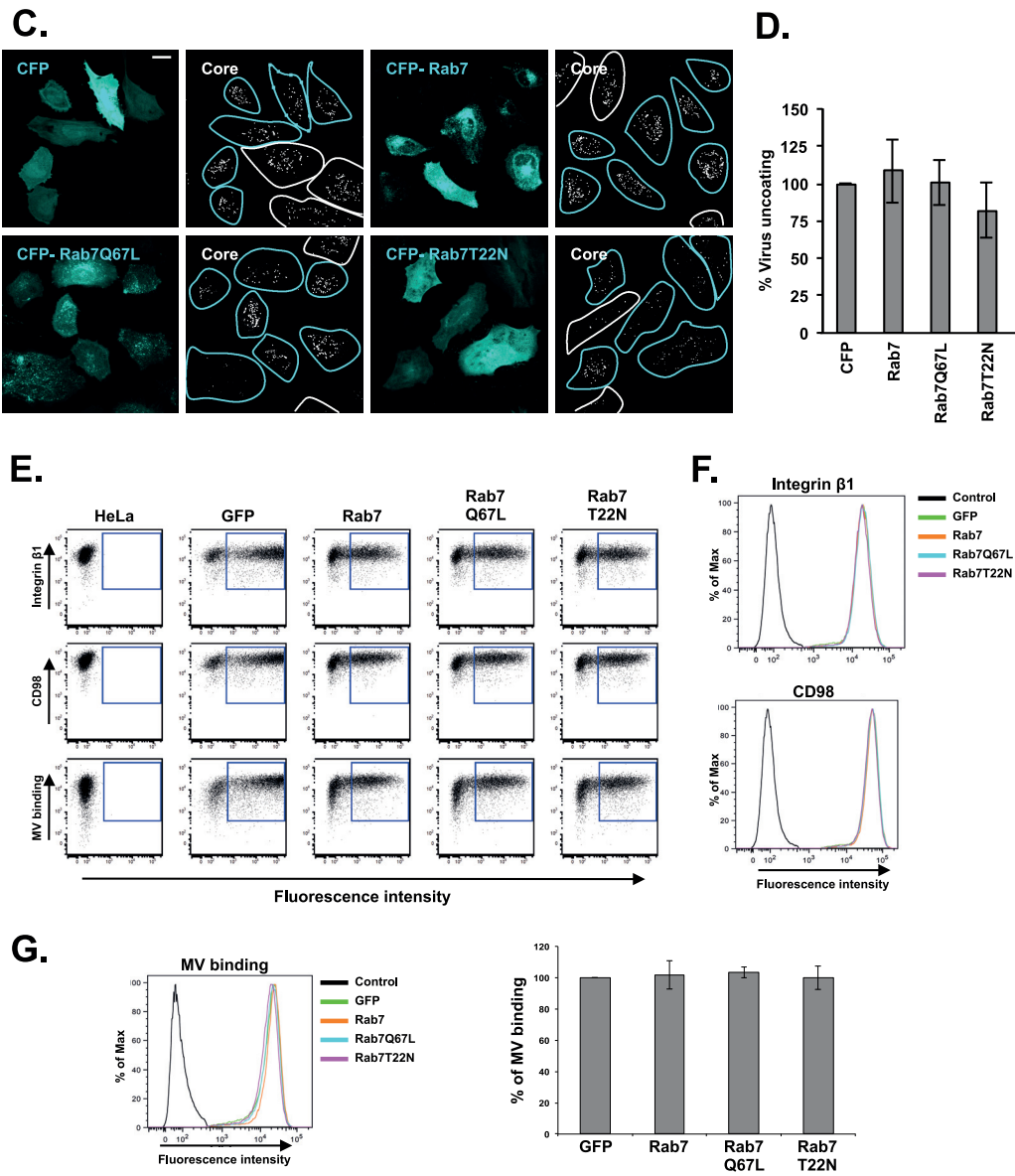


FIG 9 continued

Considering that endocytosed MV is wrapped inside vesicle membrane, it seems intuitive that the vesicle traffic pathway is dictated by the two cargo receptors that interact with vaccinia MV, integrin $\beta 1$, and CD98. Integrin $\beta 1$ was reportedly recycles back to the plasma membrane through Rab11-positive recycling endosomes (45, 47) and CD98 recycles requires Rab22-positive recycling endosomes (55, 56). Integrin $\beta 1$ also reportedly associates with CD98 on the cell surface (57, 58), so it might be interesting to know whether the recycling endosomes are double positive for Rab11 and Rab22 and whether Rab11 and Rab22 work together on MV trafficking. We attempted to answer this question by coexpressing wild type, GTP-bound, or GDP-bound forms of Rab11 and Rab22 proteins together in the same cells and determined whether vaccinia MV entry was further inhibited in these cells compared to cells expressing either Rab11 or Rab22 mutant protein. The results showed that simultaneous expression of Rab11

and Rab22 mutant proteins in the same cells did not result in more inhibition of MV entry than single mutant Rab protein expression in cells (see Fig. S4 in the supplemental material), implying that Rab11 and Rab22 may work together in the recycling pathway. Immunofluorescence staining of Rab11 and Rab22, however, did not reveal obvious colocalization of these two proteins in HeLa cells (data not shown). Although we did not label the viral membranes with fluorescent lipid dye to visualize direct viral membrane fusion with recycling endosomes in cells, the data presented through the functional interference of Rab protein activity in cells strongly support that functions of Rab11 and Rab22 proteins are important for MV entry prior to viral membrane fusion and viral core uncoating.

Our findings excluded the involvement of the late endosome/lysosome pathway in MV entry in HeLa cells, since the virus particle tracking showed a very low frequency of MV particles colo-

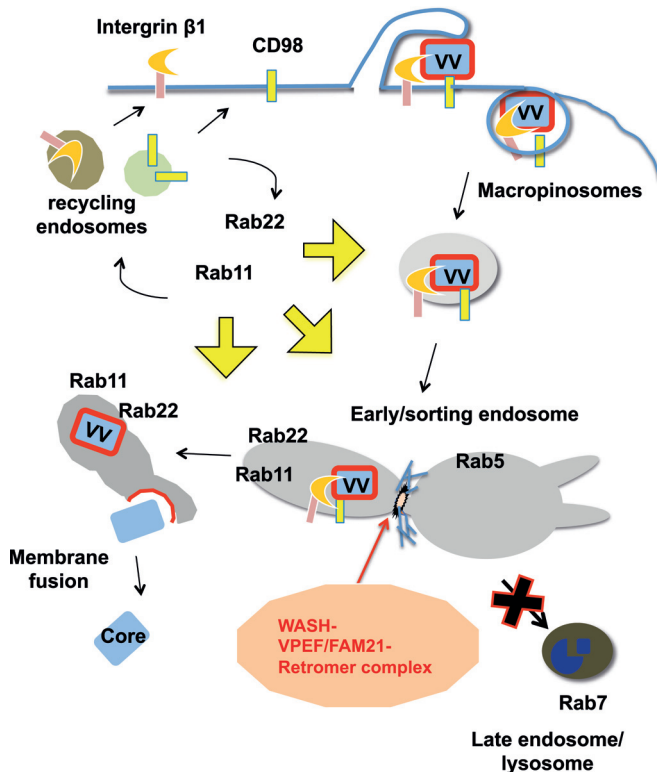


FIG 10 Intracellular trafficking of vaccinia WT-WR MV in HeLa cells. Vaccinia WT-WR MV binds to integrin $\beta 1$ (18) and CD98 (19) in lipid rafts (17) on the plasma membrane. After fluid phase endocytosis into cells, the virus-containing macropinosome traffics to the early endosome (19). There, the actions of the tethering WASH-VPEF/FAM21-retromer protein complexes mediate endosome fission and sorting of virus-containing vesicles to Rab11- and Rab22-positive recycling endosome, subsequently leading to virus membrane fusion and viral core release into cytoplasm. In addition to the involvement of endosomal trafficking of MV particles, Rab11 and Rab22 may also participate in early steps of virus entry process.

calizing with Rab7-positive late endosomes and lysosomes. In addition, the expression of Rab7-dominant mutants did not reduce WT-WR MV core release. A previous report showed that GTPase Rab34 promotes macropinosome formation (49); however, our data did not support a role of Rab34 in vaccinia virus entry in HeLa cells. ARF6 was also previously shown to regulate the trafficking of cargo receptors through the endocytic pathway in mammalian cells, but our results showed no evidence of ARF6 involvement in vaccinia MV entry (data not shown). Vaccinia MV entry differs based on the virus strain and the cell type, so it must be emphasized that our conclusions are based on results in HeLa cells and have not yet been investigated in other cell types.

We also previously showed that the cellular protein VPEF is required for WR-MV entry in HeLa cells (20). At that time, very little was known about the function of VPEF; although we initially hypothesized that VPEF may act as a cell surface molecule (38), immunofluorescence staining suggested it may play a role in vesicle transport (20). We showed here that VPEF does not work alone. The VPEF-associated WASH protein, which controls actin polymerization at endosomes (37, 40, 59), was found to be necessary for endosomal sorting of MV-containing vesicles. Furthermore, the VPEF-associated retromer complex Vps26/29/35 (59, 60) was also required for WT-MV-containing endosome sorting.

Although the retromer was initially thought to regulate endosome-to-Golgi retrieval, WASH-retromer interaction was recently shown to mediate endosome-to-plasma membrane recycling of several receptors, including integrin $\alpha 5\beta 1$ and $\beta 2$ adrenergic receptor (33, 61). It is worth noting that some components of WASH complex—such as KIAA1033, KIAA0196, Hsp70(A8 and 1A), and CCD53—remain uncharacterized and did not appear to be involved in the vaccinia MV entry process. Overall, our results extended our knowledge of vaccinia virus entry and revealed an important role of VPEF-WASH-retromer protein complexes in controlling MV sorting through early endosomes.

Each type of enveloped virus has evolved a distinct trafficking pathway during virus entry. Influenza virus (62) reportedly goes through the early endosome to the late endosome for membrane fusion, whereas hepatitis C virus (63) and VSV (64) require delivery to early endosomes but not late endosomes. Our data showed that the vaccinia mature virus trafficked to early endosomes, where it—through the aid of WASH-VPEF-retromer complexes—became further sorted to recycling endosomes, followed by membrane fusion and virus core release to the cytoplasm. Our results raise a puzzling question regarding the relationship between acidity and vaccinia MV membrane fusion (5, 65), which warrants further study to understand the physiological environments for virus membrane fusion to occur in cells.

ACKNOWLEDGMENTS

We thank Marino Zerial, Julie Donaldson, Mitsuaki Tabuchi, and Takeshi Endo for providing the plasmids. We also thank the Imaging Core Facility of the Institute of Molecular Biology at Academia Sinica for help with confocal microscopy.

This study was supported by grants from the Academia Sinica and National Science Council (NSC 101-2320-B-001-023-MY3) to W.C. and by grants from the Ministry of Education, Aim for the Top University Plan (103AC-T607), and the National Science Council (NSC 102-2320-B-010-018, MOST 103-2320-B-010-023-MY3) to Y.-H.P.

REFERENCES

- Condit RC, Moussatche N, Traktman P. 2006. In a nutshell: structure and assembly of the vaccinia virion. *Adv Virus Res* 66:31–124.
- Chung CS, Chen CH, Ho MY, Huang CY, Liao CL, Chang W. 2006. Vaccinia virus proteome: identification of proteins in vaccinia virus intracellular mature virion particles. *J Virol* 80:2127–2140. <http://dx.doi.org/10.1128/JVI.80.5.2127-2140.2006>.
- Resch W, Hixson KK, Moore RJ, Lipton MS, Moss B. 2007. Protein composition of the vaccinia virus mature virion. *Virology* 358:233–247. <http://dx.doi.org/10.1016/j.virol.2006.08.025>.
- Gong SC, Lai CF, Esteban M. 1990. Vaccinia virus induces cell fusion at acid pH and this activity is mediated by the N terminus of the 14-kDa virus envelope protein. *Virology* 178:81–91. [http://dx.doi.org/10.1016/0042-6822\(90\)90381-Z](http://dx.doi.org/10.1016/0042-6822(90)90381-Z).
- Townsley AC, Weisberg AS, Wagenaar TR, Moss B. 2006. Vaccinia virus entry into cells via a low-pH-dependent endosomal pathway. *J Virol* 80: 8899–8908. <http://dx.doi.org/10.1128/JVI.01053-06>.
- Armstrong JA, Metz DH, Young MR. 1973. The mode of entry of vaccinia virus into L cells. *J Gen Virol* 21:533–537. <http://dx.doi.org/10.1099/0022-1317-21-3-533>.
- Carter GC, Law M, Hollinshead M, Smith GL. 2005. Entry of the vaccinia virus intracellular mature virion and its interactions with glycosaminoglycans. *J Gen Virol* 86:1279–1290. <http://dx.doi.org/10.1099/vir.0.80831-0>.
- Chang A, Metz DH. 1976. Further investigations on the mode of entry of vaccinia virus into cells. *J Gen Virol* 32:275–282. <http://dx.doi.org/10.1099/0022-1317-32-2-275>.
- Doms RW, Blumenthal R, Moss B. 1990. Fusion of intra- and extracellular

- lular forms of vaccinia virus with the cell membrane. *J Virol* 64:4884–4892.
10. Krijnse Locker J, Kuehn A, Schleich S, Rutter G, Hohenberg H, Wepf R, Griffiths G. 2000. Entry of the two infectious forms of vaccinia virus at the plasma membrane is signaling-dependent for the IMV but not the EEV. *Mol Biol Cell* 11:2497–2511. <http://dx.doi.org/10.1093/mbc.11.7.2497>.
 11. Vanderplasschen A, Hollinshead M, Smith GL. 1998. Intracellular and extracellular vaccinia virions enter cells by different mechanisms. *J Gen Virol* 79(Pt 4):877–887.
 12. Bengali Z, Satheshkumar PS, Moss B. 2012. Orthopoxvirus species and strain differences in cell entry. *Virology* 433:506–512. <http://dx.doi.org/10.1016/j.virol.2012.08.044>.
 13. Chung CS, Hsiao JC, Chang YS, Chang W. 1998. A27L protein mediates vaccinia virus interaction with cell surface heparan sulfate. *J Virol* 72: 1577–1585.
 14. Hsiao J-C, Chung C-S, Chang W. 1999. Vaccinia envelope D8L protein binds to cell surface chondroitin sulfate and mediates intracellular mature virions adsorption to cells. *J Virol* 73:8750–8761.
 15. Lin CL, Chung CS, Heine HG, Chang W. 2000. Vaccinia virus envelope H3L protein binds to cell surface heparan sulfate and is important for intracellular mature virion morphogenesis and virus infection in vitro and in vivo. *J Virol* 74:3353–3365. <http://dx.doi.org/10.1128/JVI.74.7.3353-3365.2000>.
 16. Chiu WL, Lin CL, Yang MH, Tzou DL, Chang W. 2007. Vaccinia virus 4c (A26L) protein on intracellular mature virus binds to the extracellular cellular matrix laminin. *J Virol* 81:2149–2157. <http://dx.doi.org/10.1128/JVI.02302-06>.
 17. Chung CS, Huang CY, Chang W. 2005. Vaccinia virus penetration requires cholesterol and results in specific viral envelope proteins associated with lipid rafts. *J Virol* 79:1623–1634. <http://dx.doi.org/10.1128/JVI.79.3.1623-1634.2005>.
 18. Izmailyan R, Hsiao JC, Chung CS, Chen CH, Hsu PW, Liao CL, Chang W. 2012. Integrin β 1 mediates vaccinia virus entry through activation of PI3K/Akt signaling. *J Virol* 86:6677–6687. <http://dx.doi.org/10.1128/JVI.06860-11>.
 19. Schroeder N, Chung CS, Chen CH, Liao CL, Chang W. 2012. The lipid raft-associated protein CD98 is required for vaccinia virus endocytosis. *J Virol* 86:4868–4882. <http://dx.doi.org/10.1128/JVI.06610-11>.
 20. Huang CY, Lu TY, Bair CH, Chang YS, Jwo JK, Chang W. 2008. A novel cellular protein, VPEF, facilitates vaccinia virus penetration into HeLa cells through fluid phase endocytosis. *J Virol* 82:7988–7999. <http://dx.doi.org/10.1128/JVI.00894-08>.
 21. Mercer J, Helenius A. 2008. Vaccinia virus uses macropinocytosis and apoptotic mimicry to enter host cells. *Science* 320:531–535. <http://dx.doi.org/10.1126/science.1155164>.
 22. Mercer J, Helenius A. 2010. Apoptotic mimicry: phosphatidylserine-mediated macropinocytosis of vaccinia virus. *Ann N Y Acad Sci* 1209:49–55. <http://dx.doi.org/10.1111/j.1749-6632.2010.05772.x>.
 23. Laliberte JP, Moss B. 2009. Appraising the apoptotic mimicry model and the role of phospholipids for poxvirus entry. *Proc Natl Acad Sci U S A* 106:17517–17521. <http://dx.doi.org/10.1073/pnas.0909376106>.
 24. Morizono K, Xie Y, Olafsen T, Lee B, Dasgupta A, Wu AM, Chen IS. 2011. The soluble serum protein Gas6 bridges virion envelope phosphatidylserine to the TAM receptor tyrosine kinase Axl to mediate viral entry. *Cell Host Microbe* 9:286–298. <http://dx.doi.org/10.1016/j.chom.2011.03.012>.
 25. Mercer J. 2011. Viral apoptotic mimicry party: P.S. Bring your own Gas6. *Cell Host Microbe* 9:255–257. <http://dx.doi.org/10.1016/j.chom.2011.04.002>.
 26. Mazzon M, Mercer J. 2014. Lipid interactions during virus entry and infection. *Cell Microbiol* 16:1493–1502. <http://dx.doi.org/10.1111/cmi.12340>.
 27. Chang SJ, Chang YX, Izmailyan R, Tang YL, Chang W. 2010. Vaccinia virus A25 and A26 proteins are fusion suppressors for mature virions and determine strain-specific virus entry pathways into HeLa, CHO-K1, and L cells. *J Virol* 84:8422–8432. <http://dx.doi.org/10.1128/JVI.00599-10>.
 28. Joklik WK. 1962. The purification of four strains of poxvirus. *Virology* 18:9–18. [http://dx.doi.org/10.1016/0042-6822\(62\)90172-1](http://dx.doi.org/10.1016/0042-6822(62)90172-1).
 29. Tabuchi M, Yanatori I, Kawai Y, Kishi F. 2010. Retromer-mediated direct sorting is required for proper endosomal recycling of the mammalian iron transporter DMT1. *J Cell Sci* 123:756–766. <http://dx.doi.org/10.1242/jcs.060574>.
 30. Cantalupo G, Alifano P, Roberti V, Bruni CB, Bucci C. 2001. Rab-interacting lysosomal protein (RILP): the Rab7 effector required for transport to lysosomes. *EMBO J* 20:683–693. <http://dx.doi.org/10.1093/emboj/20.4.683>.
 31. Wilcke M, Johannes L, Galli T, Mayau V, Goud B, Salamero J. 2000. Rab11 regulates the compartmentalization of early endosomes required for efficient transport from early endosomes to the trans-Golgi network. *J Cell Biol* 151:1207–1220. <http://dx.doi.org/10.1083/jcb.151.6.1207>.
 32. Gullapalli A, Wolfe BL, Griffin CT, Magnuson T, Trejo J. 2006. An essential role for SNX1 in lysosomal sorting of protease-activated receptor-1: evidence for retromer-, Hrs-, and Tsg101-independent functions of sorting nexins. *Mol Biol Cell* 17:1228–1238.
 33. Zech T, Calaminus SD, Caswell P, Spence HJ, Carnell M, Insall RH, Norman J, Machesky LM. 2011. The Arp2/3 activator WASH regulates α 5 β 1-integrin-mediated invasive migration. *J Cell Sci* 124:3753–3759. <http://dx.doi.org/10.1242/jcs.080986>.
 34. Chu LW, Huang YL, Lee JH, Huang LY, Chen WJ, Lin YH, Chen JY, Xiang R, Lee CH, Ping YH. 2014. Single-virus tracking approach to reveal the interaction of dengue virus with autophagy during the early stage of infection. *J Biomed Opt* 19:011018. <http://dx.doi.org/10.1117/1.JBO.19.1.011018>.
 35. Rogers SS, Waigh TA, Zhao X, Lu JR. 2007. Precise particle tracking against a complicated background: polynomial fitting with Gaussian weight. *Phys Biol* 4:220–227. <http://dx.doi.org/10.1088/1478-3975/4/3/008>.
 36. Senkevich TG, Ward BM, Moss B. 2004. Vaccinia virus entry into cells is dependent on a virion surface protein encoded by the A28L gene. *J Virol* 78:2357–2366. <http://dx.doi.org/10.1128/JVI.78.5.2357-2366.2004>.
 37. Gomez TS, Billadeau DD. 2009. A FAM21-containing WASH complex regulates retromer-dependent sorting. *Dev Cell* 17:699–711. <http://dx.doi.org/10.1016/j.devcel.2009.09.009>.
 38. Chang W, Hsiao JC, Chung CS, Bair CH. 1995. Isolation of a monoclonal antibody which blocks vaccinia virus infection. *J Virol* 69:517–522.
 39. Chang TH, Chang SJ, Hsieh FL, Ko TP, Lin CT, Ho MR, Wang I, Hsu ST, Guo RT, Chang W, Wang AH. 2013. Crystal structure of vaccinia viral A27 protein reveals a novel structure critical for its function and complex formation with A26 protein. *PLoS Pathog* 9:e1003563. <http://dx.doi.org/10.1371/journal.ppat.1003563>.
 40. Derivery E, Sousa C, Gautier JJ, Lombard B, Loew D, Gautreau A. 2009. The Arp2/3 activator WASH controls the fission of endosomes through a large multiprotein complex. *Dev Cell* 17:712–723. <http://dx.doi.org/10.1016/j.devcel.2009.09.010>.
 41. Seaman MN. 2012. The retromer complex: endosomal protein recycling and beyond. *J Cell Sci* 125:4693–4702. <http://dx.doi.org/10.1242/jcs.103440>.
 42. Gautreau A, Oguievetskaia K, Ungermann C. 2014. Function and regulation of the endosomal fusion and fission machineries. *Cold Spring Harb Perspect Biol* 6:piia016832. <http://dx.doi.org/10.1101/cshperspect.a016832>.
 43. Schlierf B, Fey GH, Hauber J, Hocke GM, Rosorius O. 2000. Rab11b is essential for recycling of transferrin to the plasma membrane. *Exp Cell Res* 259:257–265. <http://dx.doi.org/10.1006/excr.2000.4947>.
 44. Lin SX, Mallet WG, Huang AY, Maxfield FR. 2004. Endocytosed cation-independent mannose 6-phosphate receptor traffics via the endocytic recycling compartment en route to the trans-Golgi network and a subpopulation of late endosomes. *Mol Biol Cell* 15:721–733.
 45. Powelka AM, Sun J, Li J, Gao M, Shaw LM, Sonnenberg A, Hsu VW. 2004. Stimulation-dependent recycling of integrin β 1 regulated by ARF6 and Rab11. *Traffic* 5:20–36. <http://dx.doi.org/10.1111/j.1600-0854.2004.00150.x>.
 46. Schwartz SL, Cao C, Pylypenko O, Rak A, Wandinger-Ness A. 2007. Rab GTPases at a glance. *J Cell Sci* 120:3905–3910. <http://dx.doi.org/10.1242/jcs.015909>.
 47. Eva R, Dassie E, Caswell PT, Dick G, ffrench-Constant C, Norman JC, Fawcett JW. 2010. Rab11 and its effector Rab coupling protein contribute to the trafficking of β 1 integrins during axon growth in adult dorsal root ganglion neurons and PC12 cells. *J Neurosci* 30:11654–11669. <http://dx.doi.org/10.1523/JNEUROSCI.2425-10.2010>.
 48. Eyster CA, Higginson JD, Huebner R, Porat-Shliom N, Weigert R, Wu WW, Shen RF, Donaldson JG. 2009. Discovery of new cargo proteins that enter cells through clathrin-independent endocytosis. *Traffic* 10:590–599. <http://dx.doi.org/10.1111/j.1600-0854.2009.00894.x>.
 49. Sun P, Yamamoto H, Suetsugu S, Miki H, Takenawa T, Endo T. 2003. Small GTPase Rab/Rab34 is associated with membrane ruffles and mac-

- ropinosomes and promotes macropinosome formation. *J Biol Chem* 278: 4063–4071. <http://dx.doi.org/10.1074/jbc.M208699200>.
50. Goldenberg NM, Grinstein S, Silverman M. 2007. Golgi-bound Rab34 is a novel member of the secretory pathway. *Mol Biol Cell* 18:4762–4771. <http://dx.doi.org/10.1091/mbc.E06-11-0991>.
 51. Dales S, Kajioka R. 1964. The cycle of multiplication of vaccinia virus in Earle's strain L cells. I. Uptake and penetration. *Virology* 24:278–294.
 52. Bengali Z, Townsley AC, Moss B. 2009. Vaccinia virus strain differences in cell attachment and entry. *Virology* 389:132–140. <http://dx.doi.org/10.1016/j.virol.2009.04.012>.
 53. de Magalhaes JC, Andrade AA, Silva PN, Sousa LP, Ropert C, Ferreira PC, Kroon EG, Gazzinelli RT, Bonjardim CA. 2001. A mitogenic signal triggered at an early stage of vaccinia virus infection: implication of MEK/ERK and protein kinase A in virus multiplication. *J Biol Chem* 276:38353–38360. <http://dx.doi.org/10.1074/jbc.M100183200>.
 54. Rahbar R, Murooka TT, Hinek AA, Galligan CL, Sassano A, Yu C, Srivastava K, Platanias LC, Fish EN. 2006. Vaccinia virus activation of CCR5 invokes tyrosine phosphorylation signaling events that support virus replication. *J Virol* 80:7245–7259. <http://dx.doi.org/10.1128/JVI.00463-06>.
 55. Maldonado-Baez L, Donaldson JG. 2013. Hook1, microtubules, and Rab22: mediators of selective sorting of clathrin-independent endocytic cargo proteins on endosomes. *Bioarchitecture* 3:141–146. <http://dx.doi.org/10.4161/bioa.26638>.
 56. Maldonado-Baez L, Cole NB, Kramer H, Donaldson JG. 2013. Microtubule-dependent endosomal sorting of clathrin-independent cargo by Hook1. *J Cell Biol* 201:233–247. <http://dx.doi.org/10.1083/jcb.201208172>.
 57. Fernald CC, Nishiya N, Fenczik CA, Stuhlmann H, Slepak M, Ginsberg MH. 2005. CD98hc (SLC3A2) mediates integrin signaling. *Proc Natl Acad Sci U S A* 102:355–360. <http://dx.doi.org/10.1073/pnas.0404852102>.
 58. Kim SM, Hahn JH. 2008. CD98 activation increases surface expression and clustering of $\beta 1$ integrins in MCF-7 cells through FAK/Src- and cytoskeleton-independent mechanisms. *Exp Mol Med* 40:261–270. <http://dx.doi.org/10.3858/emm.2008.40.3.261>.
 59. Jia D, Gomez TS, Billadeau DD, Rosen MK. 2012. Multiple repeat elements within the FAM21 tail link the WASH actin regulatory complex to the retromer. *Mol Biol Cell* 23:2352–2361. <http://dx.doi.org/10.1091/mbc.E11-12-1059>.
 60. Harbour ME, Breusegem SY, Seaman MN. 2012. Recruitment of the endosomal WASH complex is mediated by the extended 'tail' of Fam21 binding to the retromer protein Vps35. *Biochem J* 442:209–220. <http://dx.doi.org/10.1042/BJ20111761>.
 61. Temkin P, Lauffer B, Jager S, Cimermancic P, Krogan NJ, von Zastrow M. 2011. SNX27 mediates retromer tubule entry and endosome-to-plasma membrane trafficking of signaling receptors. *Nat Cell Biol* 13:715–721. <http://dx.doi.org/10.1038/ncb2252>.
 62. Sieczkarski SB, Whittaker GR. 2003. Differential requirements of Rab5 and Rab7 for endocytosis of influenza and other enveloped viruses. *Traffic* 4:333–343. <http://dx.doi.org/10.1034/j.1600-0854.2003.00090.x>.
 63. Meertens L, Bertaux C, Dragic T. 2006. Hepatitis C virus entry requires a critical postinternalization step and delivery to early endosomes via clathrin-coated vesicles. *J Virol* 80:11571–11578. <http://dx.doi.org/10.1128/JVI.01717-06>.
 64. Mire CE, White JM, Whitt MA. 2010. A spatio-temporal analysis of matrix protein and nucleocapsid trafficking during vesicular stomatitis virus uncoating. *PLoS Pathog* 6:e1000994. <http://dx.doi.org/10.1371/journal.ppat.1000994>.
 65. Townsley AC, Moss B. 2007. Two distinct low-pH steps promote entry of vaccinia virus. *J Virol* 81:8613–8620. <http://dx.doi.org/10.1128/JVI.00606-07>.